MDM2 Inhibition in Combination with Endocrine Therapy and CDK4/6 Inhibition for the Treatment of ER-Positive Breast Cancer.

Authors and Affiliations:

Neil Portman[1,2,†], Heloisa H. Milioli[1,2,†], Sarah Alexandrou[1,2], Rhiannon Coulson[1,3], Aliza Yong[1], Kristine J. Fernandez[1], Kee Ming Chia[1], Ensar Halilovic[4], Davendra Segara[1,2], Andrew Parker[1,2], Sue Haupt[3], Ygal Haupt[3], Wayne D. Tilley[5], Alex Swarbrick[1,2], C. Elizabeth Caldon[1,2,†] and Elgene Lim[1,2,*,†]

[1]Garvan Institute of Medical Research, Darlinghurst, Sydney, NSW 2010, Australia

[2]St. Vincent's Clinical School, Faculty of Medicine, University of New South Wales Sydney, Sydney, NSW 2010, Australia

[3]Tumor Suppression Laboratory, Peter MacCallum Cancer Centre, 305 Grattan St, Melbourne, Victoria, Australia, 3000; Sir Peter MacCallum Department of Oncology, The University of Melbourne, Parkville, Victoria 3010, Australia.

[4]Novartis Institutes of Biomedical Research, Cambridge, Massachusetts

[5]Adelaide Medical School, The University of Adelaide, SA 5001, Australia

*To whom correspondence should be addressed.

†These authors contributed equally

Running Title: MDM2 Inhibition for the Treatment of ER-Positive Breast Cancer

Keywords: Breast cancer, MDM2, Estrogen receptor, CDK4/6 inhibitor, p53.

Corresponding Author: A/Prof Elgene Lim. Garvan Institute of Medical Research, 384 Victoria St., Darlinghurst, New South Wales, 2010. Australia. Email e.lim@garvan.org.au.

Abstract:

Background: Resistance to endocrine therapy is a major clinical challenge in the management of estrogen receptor (ER)-positive breast cancer. In this setting p53 is frequently wildtype and its activity may be suppressed via upregulation of its key regulator MDM2. This underlies our rationale to evaluate MDM2 inhibition as a therapeutic strategy in treatment resistant ER-positive breast cancer.

Methods: We used the MDM2 inhibitor NVP-CGM097 to treat *in vitro* and *in vivo* models alone and in combination with fulvestrant or palbociclib. We perform cell viability, cell cycle, apoptosis and senescence assays to evaluate antitumor effects in p53 wildtype and p53 mutant ER positive cell lines (MCF-7, ZR75-1, T-47D) and MCF-7 lines resistant to endocrine therapy and to CDK4/6 inhibition. We further assess the drug effects in patient-derived xenograft (PDX) models of endocrine-sensitive and -resistant ER positive breast cancer.

Results: We demonstrate that MDM2 inhibition results in cell cycle arrest and increased apoptosis in p53-wildtype *in vitro* and *in vivo* breast cancer models, leading to potent anti-tumour activity. We find that endocrine therapy or CDK4/6 inhibition synergises with MDM2 inhibition but does not further enhance apoptosis. Instead, combination treatments result in profound regulation of cell cycle-related transcriptional programmes, with synergy achieved through increased antagonism of cell cycle progression. Combination therapy pushes cell lines resistant to fulvestrant or palbociclib to become senescent and significantly reduces tumour growth in a fulvestrant resistant patient derived xenograft model.

Conclusions: We conclude that MDM2 inhibitors in combination with ER degraders or CDK4/6 inhibitors represent a rational strategy for treating advanced, endocrine resistant ER-positive breast cancer, operating through synergistic activation of cell cycle co-regulatory programs.

Background

Estrogen receptor (ER) positive breast cancer accounts for ~ 70% of breast cancer diagnoses. For many patients, the disease is treated effectively by surgery and adjuvant endocrine therapy. Unfortunately, ~35% of patients receiving endocrine therapy relapse with resistant disease, either through inherent resistance to treatment or the emergence of acquired endocrine resistance (1, 2). Resistant disease that retains ER positivity is typically managed by treating with additional lines of endocrine therapy. Recently, the addition of Cyclin Dependent Kinase 4 and 6 (CDK4/6) inhibitors to endocrine therapy has become the new standard of care for first and second line treatment for advanced breast cancer (3). However, even with the addition of CDK4/6 inhibitors, resistance develops on average within 2-3 years and the need to identify novel targets and therapies in the resistant setting remains pressing (3, 4).

When functioning normally, p53 is activated in response to diverse genotoxic stimuli and initiates transcriptional programmes that lead to cell cycle inhibition, DNA repair and in the case of irreversible damage, apoptosis. In ER positive breast cancer and liposarcoma, the incidence of p53 mutation is relatively low (5) but there is an increased incidence of dysregulation of the major p53 regulatory proteins, MDM2 and MDM4 (6). MDM2 and MDM4 interact directly with p53 to inhibit its transcriptional activity and promote its relocation to the cytoplasm. MDM2 additionally ubiquitinates p53 to initiate its proteosomal degradation (7-10). Consequently the pharmacological reactivation of p53 function through the inhibition of MDM2 has attracted significant attention as a potential therapeutic strategy (5).

In breast cancer, although the incidence of amplification or mutation of *MDM2* is relatively low, increased abundance of MDM2 protein occurs in ~38% of all breast cancers and is more frequent among ER-positive than in ER-negative tumours (6, 11). There is significant interaction between the MDM2/p53 axis and ER signalling. *MDM2* is a transcriptional target of ER, and MDM2 protein interacts directly with ER (12, 13). ER also regulates and interacts with p53 (14, 15) and

activation of ER by either its cognate ligand or by selective ER modulators such as tamoxifen inhibits the activity of p53 (14). Simultaneous inhibition of the MDM2/p53 interaction using small molecule inhibitors, and degradation of ER via the selective estrogen receptor degrader fulvestrant can synergistically reduce proliferation of cell line models and xenografts (14, 16). Curiously, this synergy occurs without the significant induction of apoptosis (16). An unresolved question is how MDM2 inhibition synergises with endocrine therapy, and whether outcomes would be improved in combination with the new standard-of-care treatment, CDK4/6 inhibitors.

In this study, we characterised the anti-tumour effect of p53 activation via MDM2 inhibition using the small molecule inhibitor NVP-CGM097 - a dihydroisoquinolinone derivative currently being evaluated in a phase I clinical trial (17, 18) - in endocrine-resistant and endocrine-sensitive *in vitro* and *in vivo* models of ER-positive breast cancer. We show synergistic tumour cell inhibition *in vitro* in combination with either fulvestrant or palbociclib specifically via cell cycle arrest pathways, rather than by a general upregulation of p53 activity that includes apoptosis. We then demonstrate that in endocrine- and CDK4/6 inhibitor-resistant *in vitro* models, MDM2 inhibition is potentiated by combination with endocrine therapy or CDK4/6 inhibition and that this occurs via an increase in senescence compared to MDM2 inhibition alone.

Methods

Cell culture and reagents

MCF7 cells (Michigan Cancer Foundation), T-47D and ZR75-1 cells (American Type Culture Collection) lines were verified through short tandem repeat profiling and tested negative for mycoplasma contamination at the commencement of the project. Frozen stocks of each line used were generated at the commencement of the project and defrosted cells were cultured for between 10 and 20 passages. Parental cell lines were cultured in RPMI 1640 media (Thermo Fisher)

74 supplemented with 10% fetal bovine serum (GE Healthcare) and 20 mM HEPES (Thermo Fisher).
75 Fulvestrant resistant (FasR) and palbociclib resistant (PalbR). MCF-7 derivatives were developed
76 and cultured in phenol red-free RPMI 1640 (Thermo Fisher) supplemented with 5% charcoal
77 stripped fetal bovine serum (GE Healthcare), 20 mM HEPES and 10pM 17β-estradiol (Sigma).
78 Resistance to fulvestrant was developed by the continuous addition of 100nM fulvestrant (Assay
79 Matrix) over 12 months until the cells proliferated with a constant doubling time, and cells were
80 subsequently maintained with 100nM fulvestrant. Resistance to palbociclib was developed by the
81 addition of 500nM palbociclib (Selleckchem) for 8 months until the cells proliferated with a
82 constant doubling time, and cells were subsequently maintained with 500nM palbociclib. For
83 experiments that required a no-drug treatment arm, selection was removed for 48 hours prior to
84 commencement of treatment. Stock solutions of each drug (10,000x) were prepared in DMSO
85 (NVP-CGM097, fulvestrant), ethanol (17β-estradiol) or water (palbociclib). All cells were
86 cultured under 5% CO_2 in a humidified incubator at 37°C.
87
88 **Western blot analysis**
89 All Western blot analyses were repeated on at least three separate occasions using independently
90 generated lysates. Cells were lysed in RIPA buffer supplemented with Halt Protease and
91 Phosphatase Inhibitor Cocktail (Thermo Fisher). Protein lysates were separated by electrophoresis
92 over 4–15% mini-Protean TGX gels (Bio-Rad) and transferred to 0.45µm Immobilon-FL
93 polyvinylidene fluoride membrane (Millipore). Proteins were detected by immunoblotting with
94 specific primary antibodies and subsequent detection by fluorescent conjugated secondary
95 antibodies [IRDye 680RD Donkey anti-mouse (#926-68072, LI-COR) or IRDye 800CW Donkey
96 anti-Rabbit (#926-32213, LI-COR)]. Fluorescent signals were visualised using the Odyssey CLx
97 Imaging System (LI-COR). Anti-p21 12D1 (2947) and anti-p53 (9282) were sourced from Cell
98 Signalling, anti-MDM2 2A10 (ab16895) was sourced from Abcam.

99

100 **Proliferation assays**

101 Cells were seeded into 96 well plates at a density of 3000 cells in 100µl media per well. Treatment
102 was delivered via replacement of the media in each well with fresh media containing the indicated
103 concentrations of drugs the following day. Mitochondrial activity (as an indication of cell viability)
104 was assessed using the alamar blue assay (Thermo Fisher) according to the manufacturer's
105 instructions two days after treatment. Experiments were performed in three independent replicates.
106 Growth inhibition was calculated using the formula $1 - \left(\frac{treated}{vehicle}\right)$. Alternatively, proliferation
107 was measured by cell number using the IncucyteTM live-cell imaging system (Essen Bioscience).
108 Cells were plated at 1000-3000 cells per well in a 96 well plate in 40 wells/cell line, and cell
109 number determined by imaging every 1-2 days for 2 weeks. IC50 values were calculated from non-
110 linear regression analyses performed in GraphPad Prism (version 7.04, GraphPad Software).
111 Synergy was quantified using a dose-effect approach with a constant dose ratio design as per Chou
112 and Talalay (19). Combination Indices (C.I.) were calculated using CompuSyn software
113 (ComboSyn, Inc) such that a $\log_2$(C.I.) < 0 indicates synergy.

114

115 **Senescence assay**

116 Senescence was assayed by visualising β-galactosidase activity using Senescence β-galactosidase
117 staining kit (Cell Signalling) according to the manufacturer's instructions. Three fields of
118 approximately 100 cells were scored for each of three independent replicates for each treatment
119 condition.

120

121 **Flow cytometry**

122 Flow cytometry was performed on a Becton Dickinson CantoII flow cytometer using BD
123 FACSDIVA software, and the results were analysed using Flowjo software (Tree Star Inc.). Cells

124 were treated with 10nM Bromo-deoxyuridine (BrdU) for two hours prior to harvest by addition of
125 trypsin. BrdU was detected using FITC-conjugated anti-BrdU (BD Bioscience) according to the
126 manufacturer's protocol. Total DNA was detected by co-staining with Propidium Iodide (PI). For
127 quantification of apoptosis, cells were assessed using the APC AnnexinV Apoptosis Detection Kit
128 with PI (BioLegend, CA, USA; #640932) as per the manufacturer's instructions. Between 5000
129 and 10000 cells were analysed per sample and each experiment was conducted in triplicate.
130

131 **Patient-derived breast cancer xenograft (PDX) models**

132 All *in vivo* experiments, procedures and endpoints were approved by the Garvan Institute of
133 Medical Research Animal Ethics Committee (protocol 15/25). KCC_P_3837
134 (HREC/13/RPA/187) was derived from an untreated grade 3, ER-positive, PR-positive, HER2-
135 negative primary invasive ductal carcinoma. Gar15-13 (#14002, HREC/H2006/2633) was resected
136 from a breast cancer liver metastasis of an endocrine resistant ER-positive, PR-negative, HER2-
137 negative metastatic breast cancer (20). At surgery, 4mm^3 sections of tumour tissue were implanted
138 into the 4th inguinal mammary gland of 6-8 week old female NOD-SCID-IL2γR-/- mice
139 (Australian BioResources Pty Ltd) (21). For KCC_P_3837, tumour growth was supported by
140 implantation of a silastic pellet containing 0.72mg 17β-estradiol. Tumour growth was assessed
141 twice weekly by caliper measurement and mice were randomized to treatment arms when tumours
142 reached 150-250mm^3 (using the formula: $width^2 \times length \times 0.5$) using an online randomisation
143 tool (https://www.graphpad.com/quickcalcs/randomize1.cfm). 100mg/kg NVP-CGM097
144 (20mg/ml in 2% DMSO) was administered by oral gavage 5 days a week. 5mg/body fulvestrant
145 (50mg/ml in peanut oil – Sigma P2144) was delivered by sub-cutaneous injection once per week.
146 Mice were treated for 60 days or until tumour volume reached 1000mm^3.
147

148 **Immunohistochemistry (IHC) and quantification**

149 Tumour tissue was harvested and immediately fixed in 10% neutral buffered formalin at 4ºC
150 overnight before dehydration and paraffin embedding. Antibodies used for IHC were anti-ER
151 (M7047, 1:300, Agilent) and anti-Ki67 (M7240, 1:400, Agilent). Primary antibodies were detected
152 using biotinylated IgG secondary antibodies (Agilent, 1:400), using streptavidin-HRP (Agilent)
153 for amplification of signal followed by the addition of 3,3'-diaminobenzidine (Sigma) substrate.
154 Images were scanned using Leica Aperio Slide Scanner (Leica Biosystems) and analysed using
155 QuPath software to differentiate tumour tissue from stroma and necrosis, and to quantify Ki-67
156 positivity in tumour tissue.
157

158 **Statistical Analysis**

159 Statistical analyses were performed in GraphPad Prism (version 7.04, GraphPad Software) or in
160 Microsoft Excel (χ^2 test for cell cycle phase analysis). * = $p<0.05$, ** = $p<0.01$, *** = $p<0.001$,
161 **** = $p<0.0001$, ns = $p>=0.05$.
162

163 **Differential Expression and Gene Set Enrichment Analysis**

164 Total RNA was extracted from breast cancer cell lines and tissue samples using RNeasy Mini Kit
165 (Qiagen) following the manufacturer's instructions. For tumour tissue, snap frozen sections were
166 first disrupted in lysis buffer in a TissueLyser II (QIAGEN). Sequencing data was processed on
167 the Illumina HiSeq 2500 v4.0 System. Sequences were trimmed using Trim Galore (version 0.4.4)
168 and genome-guided alignment to a human reference (HG38) was performed using STAR software
169 (version 2.5). Feature counts were computed in R (version 3.4.3) using the package *Rsubread* (22).
170 Differential gene expression analysis was conducted with *edgeR* (23, 24) and *limma* (25) packages,
171 on a threshold of p.val < 0.05 and twofold change. The read count quantitation and normalized
172 expression matrix can be downloaded from http://www.ncbi.nlm.nih.gov/geo (GSE140758). Gene
173 set enrichment analysis (GSEA) and pathway annotation were attained using *cluterProfiler* (26)

174 in R. GSEA was tested on hallmark and curated gene sets and on gene ontology (GO) terms from
175 the Molecular Signatures Database (MSigDB), Broad Institute (http://software.broadinstitute.org).
176 Pathway enrichment was analysed in the Kyoto Encyclopedia of Genes and Genomes (KEGG)
177 database (https://www.genome.jp/kegg/pathway.html).
178

179 **Results**

180 **The small molecule MDM2 inhibitor NVP-CGM097 inhibits ER-positive breast cancer cells**
181 **in a p53-dependent manner.**

182 ER-positive primary breast cancer has a relatively low incidence of *TP53* mutation (~20%) (5). To
183 establish whether this situation is preserved in the resistant/metastatic setting, we assessed the
184 frequency of *TP53* mutation or deletion across public cohorts in the cBio Cancer Genomics Portal
185 (cBioPortal, http://cbioportal.org) (Fig. 1A). The incidence of *TP53* aberration in advanced ER-
186 positive breast cancers was ~20%, equivalent to that observed in primary tumours and relatively
187 low compared to other cancer types (International Agency for Research on Cancer, IARC)
188 database (http://p53.iarc.fr). In the same clinical datasets, no instances of *MDM2* mutation or
189 deletion were detected (data not shown). Thus, the inhibition of MDM2 to increase $p53^{wt}$ activity
190 could be a viable strategy in both primary and metastatic ER-positive breast cancer settings.

191 The MDM2 inhibitor NVP-CGM097 effectively hinders cancer cell proliferation in a $TP53^{wt}$
192 dependent manner (27-29). However, this has not been specifically demonstrated in ER-positive
193 breast cancer models and we therefore determined the effect of NVP-CGM097 on cell viability in
194 three *in vitro* models. After 48 hours of treatment, $TP53^{wt}$ MCF-7 and $TP53^{wt}$ ZR75-1 responded
195 to 1μM NVP-CGM097, exhibiting a loss of normal morphology with the adoption of stellate
196 morphology and greater separation between cells (Fig. 1B). Sub-micromolar IC_{50} concentrations
197 were measured by alamar blue assay for MCF-7, 1.78×10^{-7}M and ZR75-1, 2.05×10^{-7}M (Fig. 1C).

198 *TP53* mutant (*TP53*^{mut}) T-47D, however, showed no morphological changes after 48 hours
199 treatment with 1μM NVP-CGM097 (Fig. 1B) and exhibited an inhibitory response only at high
200 doses (IC50: 7.19x10^{-6} M) (Fig. 1C).
201

202 **MDM2 inhibition activates p53 transcriptional activity in cell line models of ER-positive**
203 **p53^{wt} breast cancer**

204 Using western blot analysis, we assessed p53 reactivation in cells treated with vehicle (0.01%
205 DMSO) or 1μM NVP-CGM097 for 48 hours (Fig. 1D, Fig. S1A). In MCF-7 and ZR75-1, p53
206 levels increased in response to treatment, consistent with successful inhibition of MDM2-mediated
207 degradation of p53 protein. The p53^{mut} produced by T-47D accumulated in both vehicle and treated
208 cells. Protein levels of the p53 transcriptional targets MDM2 and p21 were increased in MCF-7
209 and ZR75-1, but not in T-47D cell lines, after treatment. Collectively, these results indicate that
210 NVP-CGM097 acts on-target to inhibit MDM2/p53 interaction with consequent p53^{wt} stabilisation
211 and activation in models of ER-positive breast cancer.

212 We next performed RNA Sequencing (RNA Seq) on MCF-7 cell to interrogate effects on key p53
213 targets that are associated with cell cycle progression and programmed cell death (Fig. 1E).
214 Treatment of MCF-7 cells with 1μM NVP-CGM097 for 48 hours induced the expression of
215 *CDKN1A* (p21), *CCND1* (cyclin D1), *SFN* (14-3-3-σ) and *GADD45A* (Gadd45), which supports
216 the activation of molecular mechanisms involved in cell cycle arrest. MDM2 inhibition also led to
217 increased mRNA levels of apoptosis markers, including *FAS*, *BAX* (Bax), *BID* (Bid) and *BBC3*
218 (PUMA). These findings confirm NVP-CGM097-mediated p53 activation of downstream targets
219 at the molecular level in MCF-7 cell lines.
220

221 **MDM2 inhibition causes G_1 and G_2/M cell cycle arrest and apoptosis in treatment naïve**
222 **breast cancer models**

223 Given the several anti-proliferative outcomes of p53 activation, we next examined the mechanisms
224 by which MDM2 inhibition compromises cell viability. Effects on cell cycle progression were
225 assessed in MCF-7, ZR75-1 and T-47D cells after 48 hours in the presence or absence of 1μM
226 NVP-CGM097. We quantified total DNA content of individual cells and the incorporation of
227 Bromo-deoxyuridine (BrdU) over a two-hour pulse (Fig. 1F). In both MCF-7 and ZR75-1,
228 treatment with NVP-CGM097 almost completely eliminated BrdU incorporation (χ^2 $p<0.001$)
229 with concomitant decrease in the proportion of cells in S phase and an increase in the proportion
230 of cells in G_2/M (MCF-7 χ^2 $p = 0.003$; ZR75-1 χ^2 $p < 0.001$) (Fig. S1B). In T-47D cells, there was
231 no significant effect on either the incorporation of BrdU (χ^2 $p=0.70$) or on the distribution of cells
232 in the cell cycle (χ^2 $p=0.78$) after treatment with NVP-CGM097. We quantified the effect of NVP-
233 CGM097 on apoptosis in MCF-7, ZR75-1 and T-47D by staining for phosphatidylserine on the
234 cell surface using fluorescent AnnexinV. Treatment with 1μM NVP-CGM097 for 96 hours
235 significantly increased the proportion of apoptotic cells compared to vehicle treated populations
236 in both MCF-7 and ZR75-1 (MCF-7 $p<0.01$; ZR75-1 $p<0.001$) (Fig. 1G).
237 The effects of MDM2 inhibition were further validated on a $p53^{wt}$ patient derived xenograft (PDX)
238 model of endocrine-sensitive ER-positive breast cancer derived from a surgically resected primary
239 treatment-naïve ER-positive breast cancer (KCC_P_3837). Tumours were implanted concurrently
240 with estradiol pellets and once tumour volume reached 100-150mm^3 were treated with vehicle
241 (estradiol, 2% DMSO) or NVP-CGM097 (100mg/kg by daily gavage) for 60 days. NVP-CGM097
242 significantly inhibited tumour growth (Fig. 2A) and final tumour volume (Fig. S1C) relative to
243 vehicle. Immunohistological quantification of the proliferation marker Ki-67 at endpoint showed
244 a significant decrease in the proportion of Ki-67 positive cells in tumours treated with NVP-
245 CGM097 (Fig. 2B, Fig. S1D). Together, these data show that NVP-CGM097 is an effective
246 inhibitor of proliferation in breast cancer models via p53-dependent induction of apoptosis and
247 cell cycle arrest.

248

249 **The combination of NVP-CGM097 and fulvestrant synergistically inhibits MCF-7 cells**
250 **without increasing apoptosis**

251 Fulvestrant is a standard therapeutic option in the treatment of women with advanced ER-positive
252 breast cancer. We therefore combined NVP-CGM097 with fulvestrant and measured viability of
253 parental MCF-7 cells to test for an enhanced effect through drug additivity or synergy (Fig. 3A).
254 We calculated combination indices using Compusyn software and detected a significant
255 synergistic effect ($\log_2$ combination index < 0) on viability when combining the drugs (Fig. 3B).
256 We then quantified the effect of NVP-CGM097 alone and in combination with fulvestrant on the
257 rate of apoptosis in MCF-7 cells (Fig. 3C). As previously shown (Fig. 1F), treatment with 1μM
258 NVP-CGM097 for 96 hours significantly increased the proportion of apoptotic cells compared to
259 vehicle treated populations ($p<0.01$). By contrast, the inclusion of 1nM fulvestrant yielded no
260 significant additional effect, suggesting that the synergy observed in the viability assays does not
261 occur via enhancement of p53-mediated apoptosis.

262

263 **Combination of NVP-CGM097 with fulvestrant downregulates E2F and G_2/M**
264 **transcriptional programmes *in vitro***

265 To identify the molecular mechanisms underlying the combination effects of NVP-CGM097 and
266 fulvestrant we quantified the transcriptional profile of MCF-7 cells after 48 hours treatment with
267 0.01% DMSO, 1μM NVP-CGM097, 1nM fulvestrant or the combination of NVP-CGM097 and
268 fulvestrant at these doses (Fig. S2A). Under stringent thresholds (adjusted p-value<0.05- and 2-
269 fold change), 576 genes were significantly regulated by NVP-CGM097 Table S1), 803 by
270 fulvestrant (Table S2) and 1104 by combination (Table S3) compared to vehicle. Combination
271 therapy incorporated most of NVP-CGM097 (80%) and fulvestrant (90%)-induced gene
272 regulation, and further altered unique gene sets that are central players in DNA replication,

273 including the minichromosome maintenance protein complex (MCM) and DNA polymerase
274 subunits (Fig. S2B, Table S4). The involvement of these additional gene sets suggests direct and
275 indirect downstream regulation of the cell cycle machinery.
276 Kyoto Encyclopedia of Genes and Genomes (KEGG) pathway enrichment analysis of differential
277 gene expression induced by combination therapy revealed a significant negative regulation of *Cell*
278 *Cycle* (p=1.08E-21; Fig. S2C) and positive enrichment of *p53 Signalling Pathway* (p=1.95E-10;
279 Fig. S2, C and D; Table S5) compared to vehicle. NVP-CGM097 in combination with fulvestrant
280 significantly regulated a set of genes involved in intertwined signalling cascades of cell cycle,
281 apoptosis and cellular senescence (Fig. 3D; Fig. S3A). In MCF-7 cell lines, combination therapy
282 enhanced the downregulation of essential components of the cell cycle (*HMMR*, *AURKB*, *BIRC5*)
283 that control proliferative activities and tumour growth alongside downregulation of the anti-
284 senescence markers *FOXM1* and *E2F1* (30). FOXM1 also regulates the expression of G_2/M cell
285 cycle genes, including the levels of its known mitotic targets *CCNB1* and *CDC20* (31, 32). The
286 upregulation of pro-senescence markers *CDKN1A* (p21) and *CDKN2B* (p15) – master effectors of
287 multiple tumour suppressor pathways – and pro-apoptotic markers, such as *BBC3*, *BAX*, *BID* and
288 *BAK1*, also contributes to the regulation of cell homeostasis, although our *in vitro* data of
289 combination therapy indicate that synergy between treatments is not dependent on increased
290 apoptosis.
291 Gene Set Enrichment Analysis (GSEA) revealed enhanced downregulation of key hallmarks
292 involved in cell proliferation and cell cycle regulation, including E2F Targets and G_2/M
293 Checkpoint, in combination treated cells compared to either drug alone (Fig. 3E). To quantify the
294 additional effect elicited by combination therapy at the transcriptional level, we computed a score
295 for each gene x based on the log fold change compared to vehicle for each condition (Tables S1-
296 3) as follows: $Score_x = log2(Combination_x/(NVPCGM097_x + fulvestrant_x))$ (Table S6).
297 Using this formula, a score greater than 0 denotes transcripts in which the differential gene

298 expression detected for the combination treatment exceeds the sum of effect for each individual
299 treatment. Transcripts from the KEGG annotated Cell Cycle gene set were significantly over-
300 represented within the cohort scoring above 0 (Wilcoxon rank sum test $p=4.45x10^{-7}$)
301

302 **The combination of MDM2 inhibition and fulvestrant increases senescence in fulvestrant**
303 **resistant cells compared to MDM2 inhibition alone**

304 We next asked whether combining NVP-CGM097 and fulvestrant could lead to enhancement or
305 re-sensitisation to therapy in fulvestrant resistant MCF-7 (FasR) cell lines. MCF-7 FasR were
306 generated by the continuous administration of 100nM Fulvestrant for 12 months to MCF-7 cells.
307 Resistance was confirmed by examination of relative proliferation of the parental MCF-7 cells and
308 MCF-7 FasR cells using an Incucyte confluence assay (Fig. S4A). We first treated MCF-7 FasR
309 cells with escalating doses of NVP-CGM097 in the presence or absence of 100nM fulvestrant (the
310 dose used to generate fulvestrant resistance in this model) (Fig. 4A). No significant difference was
311 observed in cell viability between the two treatments using the alamar blue assay. Treatment with
312 1μM NVP-CGM097 for 48 hours significantly altered the cell cycle phase distribution of MCF-7
313 FasR cells (χ^2 $p<0.001$) resulting in a decrease in the proportion of cells in S phase, consistent with
314 our findings from parental MCF-7 cells, and no significant difference in distribution was observed
315 with the addition of 100nM fulvestrant (Fig. 4B). Increased levels of p21 protein were comparable
316 between treatment with 1μM NVP-CGM097 alone for 48 hours and after treatment in combination
317 with 100nM fulvestrant (Fig. 4C, Fig. S4B). Treatment with 100nM fulvestrant alone yielded no
318 change in p21 levels compared to untreated cells. We observed phenotypically distinct cells
319 following treatment with NVP-CGM097 alone and in combination with fulvestrant, with a
320 flattened morphology reminiscent of senescence (Fig. 4D). Consequently, we analysed the cells
321 for senescence via accumulation of senescence-associated β-galactosidase. We observed a
322 significant increase in β-galactosidase staining in cells treated with the combination of 1μM NVP-

323 CGM097 and 100nM fulvestrant for 72 hours compared to vehicle treatment or treatment with
324 either single agent alone ($p<0.01$ vs NVP-CGM097; $p<0.001$ vs fulvestrant) (Fig. 4E).
325

326 **Combination NVP-CGM097/fulvestrant reduces tumour growth in an *in vivo* PDX model of**
327 **endocrine resistance**

328 To investigate this enhancement of effect *in vivo*, we treated a $p53^{wt}$ PDX model of endocrine-
329 resistant ER-positive breast cancer, Gar15-13 (20), with vehicle (DMSO), NVP-CGM097,
330 fulvestrant or combination therapy. Gar15-13 was established from a liver metastasis progressing
331 on the aromatase inhibitor anastrozole. It maintains high ER positivity but grows independently of
332 estradiol supplementation, consistent with its prior exposure to aromatase inhibition in the patient
333 (20). This model is resistant to fulvestrant and fulvestrant-treated tumours progressed rapidly to
334 tumour volume endpoint with growth kinetics and survival outcomes similar to the vehicle arm
335 (Fig. 5A). NVP-CGM097 alone significantly inhibited tumour growth (Fig. 5A) and extended
336 survival (Fig. 5, B and C) and surprisingly, given the model's resistance to fulvestrant,
337 combination treatment reduced tumour growth (Fig, 5A) and increased survival time significantly
338 more than NVP-CGM097 alone, with benefit continuing beyond the six week period of
339 administration (Fig. 5, B and C). Gar15-13 PDX treated for ten days with NVP-CGM097 alone
340 or in combination with fulvestrant showed reduced Ki-67 staining compared to vehicle treated
341 tumours, although no significant difference was observed between the NVP-CGM097 only arm
342 and the combination arm (Vehicle vs NVP-CGM097 $p<0.01$; Vehicle vs combination $p=0.011$, all
343 other pairwise comparisons not significant at $\alpha=0.05$) (Fig. 5D). Tumours treated for ten days with
344 fulvestrant (either alone or in combination) showed a significant reduction in the intensity of ER
345 staining by immunohistochemistry in both the nucleus and cytoplasm (Vehicle vs fulvestrant -
346 nuclear ER $p=0.038$, cytoplasmic ER $p<0.01$; vehicle vs combination - nuclear ER $p=0.013$,
347 cytoplasmic ER $p<0.001$) (Fig. S4C), demonstrating efficacy of fulvestrant in targeting ER but not

348 in directly inhibiting growth. The observed enhancement of the effects of NVP-CGM097 with the
349 addition of fulvestrant may therefore be the result of an interaction with functions of ER not
350 directly associated with proliferation, for example, in the context of senescence as we have
351 demonstrated in MCF-7 FasR.
352
353 **Effects of single agent and combination therapy reconcile targeted molecular mechanisms in**
354 **both *in vitro* and *in vivo* models**
355 RNASeq analysis of short-term (10 day) treated tumours showed differential genes ($p<0.05$)
356 induced by NVP-CGM097 (n=141), fulvestrant (n=411) and combination therapy (n=484) (Table
357 S7-9). GSEA demonstrated negative enrichment of E2F Targets and G_2/M Checkpoint and other
358 relevant hallmark gene sets, including MYC Targets and p53 Pathway (Table S10-15). These
359 signatures were concurrently enriched in both *in vitro* and *in vivo* models (Fig. 5E). In Gar15-13,
360 combination therapy elicited an enhanced effect on cell cycle proliferative gene sets, E2F and
361 G_2/M (Fig. S4D and E; Table S16) compared to single agent treatments. Notably, fulvestrant
362 treatment *in vitro* or *in vivo* did not show effect on the hallmarks of p53 Pathway (Fig. 5E), which
363 was reassuringly strongly upregulated by treatment with NVP-CGM097 in both settings.
364 Combination treatment of NVP-CGM097 with fulvestrant also led to decreased expression of key
365 cell cycle markers, including *DLGAP5*, *HMMR*, *AURKB*, *BIRC5*, *BUB1* and *CDC20* (Fig. S4E),
366 which is consistent with those identified in MCF-7 treated cells. The strong inhibitory effect of
367 combination therapy on cell cycle thus provide a preclinical rationale to use MDM2 inhibitors with
368 ER degraders to enhance the therapeutic effects of endocrine sensitive and resistant ER-positive
369 $p53^{wt}$ breast cancer.
370
371 **MDM2 inhibition synergises with CDK4/6 inhibitors via the same mechanisms that underlie**
372 **synergy with fulvestrant**

373 Treatment with CDK4/6 inhibitors has become a standard of care for advanced ER positive breast
374 cancer that has failed endocrine therapy (4). CDK4/6 inhibitors act through the G_1/S axis to prevent
375 cell cycle entry and have many overlapping target genes with endocrine therapy. Consequently,
376 we investigated the potential of combination therapy of NVP-CGM097 and palbociclib, a major
377 CDK4/6 inhibitor used in clinical practice. We performed a constant dose ratio protocol with NVP-
378 CGM097 and palbociclib (Fig. 6A), followed by combination index analysis on MCF-7 cells. A
379 significant synergistic effect on viability was observed with the combination therapy compared to
380 either single agent alone (Fig. 6B).
381 We next investigated the combinatorial effect of NVP-CGM097 and palbociclib by RNA-Seq (Fig.
382 S5A). We confirmed significant (adjusted p-value<0.05- and 2-fold change) gene expression
383 changes induced by NVP-CGM097 (n=572), palbociclib (n=392) and combination therapy
384 (n=714) (S17-19), compared to vehicle (0.01% DMSO). Combination therapy encompassed about
385 90% of the changes promoted by either agent alone (Fig. S5B). Combination of NVP-CGM097
386 with fulvestrant or with palbociclib showed a significant overlap (Fig. 6C). As with NVP-CGM097
387 plus fulvestrant, when we quantified the additional effect elicited by combination therapy at the
388 transcriptional level (Table S20), transcripts from the KEGG annotated Cell Cycle gene set were
389 significantly over-represented within the cohort scoring above 0 (Wilcoxon rank sum test
390 $p=1.52x10^{-13}$). Combination of NVP-CGM097 with palbociclib further downregulates the
391 senescence gatekeepers *MYBL2*, *FOXM1, CCNB1* and *E2F1* (Fig. 6D). Although both fulvestrant
392 and palbociclib interact with the p53 pathway at numerous points, especially fulvestrant which
393 ablates the interaction between ER and p53 (14), our data suggest that the major common
394 mechanistic events underlying the efficacy of the two combination strategies with NVP-CGM097
395 are related to the activity of each drug in terms of inhibiting cell cycle progression.
396

397 **The combination of MDM2 inhibition and palbociclib increases senescence in palbociclib**
398 **resistant cells compared to MDM2 inhibition alone.**
399 We investigated the effect of MDM2 inhibition on MCF-7 cells with acquired resistance to
400 palbociclib (PalbR). MCF-7 PalbR were generated by the continuous administration of 500nM
401 palbociclib for 6 months to MCF-7 cells. Resistance was confirmed by examination of relative
402 growth inhibition of the parental MCF-7 cells and MCF-7 PalbR cells to a range of doses of
403 palbociclib (Fig. S5C). NVP-CGM097 inhibited growth of MCF-7 PalbR cells with an IC_{50} of
404 $9.0x10^{-8}$M (95% C.I. $6.7x10^{-8}$M to $1.1x10^{-7}$M), as determined by alamar blue assay (Fig. 7A).
405 Analysis of cell cycle phase by flow cytometry showed a significant difference (χ^2 $p<0.001$) in
406 distribution from vehicle (500nM palbociclib, 0.01% DMSO) following treatment for 48 hours
407 with 1μM NVP-CGM097 (Fig. 7B) with an increase in the proportion of cells in G_2/M. A key
408 difference to endocrine resistance models was that MCF-7 PalbR cells did not accumulate in G_1
409 after NVP-CGM097 treatment. This suggests that cells resistant to CDK4/6 inhibition may be
410 able to overcome the G_1 block associated with activation of p53 to some extent but are still
411 susceptible to cell cycle inhibition in S and/or G_2/M. Treatment with 1μM NVP-CGM097 for 96
412 hours resulted in a significant increase in the proportion of apoptotic cells compared to vehicle
413 (0.01% DMSO) or 500nM palbociclib treated cells ($p<0.001$) but the combination treatment
414 yielded no significant increase compared to NVP-CGM097 alone (Fig. 7C).
415 We had observed that NVP-CGM097 in combination with fulvestrant resulted in increased
416 senescence compared to NVP-CGM097 alone in fulvestrant resistant cells. We examined whether
417 a similar increase could also be observed with CDK4/6 inhibitor-resistant cells treated with
418 combination NVP-CGM097 and palbociclib. MCF-7 PalbR cells were treated with 1μM NVP-
419 CGM097 in combination with 500nM palbociclib (the resistance dose) for 48 hours. Treatment
420 with either single agent NVP-CGM097 or the combination with palbociclib increased expression
421 of the senescence marker p21 (33) (Fig. 7D, Fig S5D) and there was a significant increase in the

422 proportion of β-galactosidase positive cells in the combination treatment compared to either single
423 agent alone ($p<0.001$ vs NVP-CGM097 or palbociclib) (Fig. 7, E and F). Thus, NVP-CGM097 is
424 an effective inhibitor of ER-positive breast cancer even in the context of palbociclib resistance,
425 and as with endocrine therapy, rechallenging cells in the presence of NVP-CGM097 increases the
426 incidence of senescence compared with single agent treatments.
427

428 **Discussion**

429 The treatment of patients with endocrine-resistant ER-positive breast cancer is extremely
430 challenging, as in this setting, disease leads inevitably to death. Numerous mechanisms of
431 treatment resistance have been identified. While some of these pathways are targetable, for
432 instance, the PI3K pathway and the cyclinD-CDK4/6-Rb axis; the optimal next-line treatment
433 strategies are unclear. In this context, MDM2 inhibition to reactivate p53 is particularly attractive
434 in ER-positive breast cancer as it has a relatively low incidence of *Tp53* mutation in the primary
435 and metastatic setting (~20%) (5). In addition, those ER-positive breast cancer patients who
436 respond to CDK4/6 inhibitors are more likely to have intact p53 (34), meaning that there is the
437 potential to improve the response to CDK4/6 inhibitors through p53 activation.
438 A number of small molecule MDM2 inhibitors have been designed and are at various stages of
439 clinical development (35). NVP-CGM097 was one of the first of the new generation inhibitors and
440 has advanced to phase 1 clinical trial (NCT01760525). Although the final outcomes of the trial
441 have not yet been reported, early results showed clinical activity – predominantly stable disease –
442 and establishment of a tolerable dose regimen, with one quarter of patients receiving treatment for
443 at least 24 weeks (18). The reported Phase I dose of CGM097 was 300-700mg three times per
444 week on a 21-day cycle with two weeks on and one week off. p53 pathway activation was
445 demonstrated by the induction of its downstream target GDF-15 in serum and plasma. This aligns

446 well with the dose used in this study of 100mg/kg in mice, which converts to a human equivalent
447 dose of ~500mg for a 60kg patient (36). As with most MDM2 inhibitors that have so far reached
448 clinical trials, side effects of NVP-CGM097 include thrombocytopenia and neutropenia which
449 would need to be considered in any clinical application in combination with drugs with
450 overlapping toxicity profiles such as CDK4/6 inhibitors (37). Importantly, our data show that
451 combination of NVP-CGM097 with fulvestrant, which is not associated with hematological
452 adverse effects, has a highly similar response profile to combination with CDK4/6 inhibition in
453 terms of the key molecular pathways affected. It is currently unclear as to whether NVP-CGM097
454 itself will continue in development, however a range of next generation MDM2 inhibitors with
455 improved tolerability are in development (38). Our results demonstrate that MDM2 inhibition is a
456 rational target for novel therapeutic strategies in the setting of treatment resistant breast cancer.
457 In this study we show that reactivation of wildtype p53 using NVP-CGM097 is an effective
458 inhibitor of tumour growth in multiple models of endocrine-naïve, endocrine-resistant and
459 CDK4/6 inhibitor-resistant ER-positive breast cancer *in vitro* and *in vivo*. We identify the key
460 mechanisms of the synergistic interactions between NVP-CGM097 and endocrine therapy, which
461 occurs through the inhibition of E2F targets and G_2/M checkpoint signalling and induction of
462 senescence; rather than via a general upregulation of p53 dependent apoptotic pathways above the
463 level of MDM2 inhibition alone. Moreover, we find these same pathways are specifically targeted
464 in response to combined inhibition of both MDM2 and the CDK4/6 pathway.
465 Consistent with activation of p53, NVP-CGM097 induced apoptosis, and cell cycle arrest in G_1
466 and G_2, in *TP53*^{wt} ER-positive breast cancer cell line (MCF-7 and ZR75-1) models. The only
467 setting in which we did not observe anti-tumour effect was in the case of the *TP53*^{mut} T-47D cell
468 line model which supports our conclusion that activity of NVP-CGM097 requires wildtype p53.
469 MDM2 inhibition was characterised by very high expression of the key cell cycle regulator p21 –

470 which is a p53 target and principal component of cell cycle arrest in G_1 and G_2 and in the induction
471 and maintenance of senescence (39).
472 Our data from ER positive PDX models shows that NVP-CGM097 is effective as a single agent,
473 and it combines with fulvestrant to be highly effective in the fulvestrant-resistant Gar15-13 PDX
474 model. In the only other breast cancer PDX experiments so far reported, another MDM2 inhibitor
475 MI-77301 was effective at reducing tumour growth of two fulvestrant-resistant PDX models (16).
476 Similar to our findings, co-administration of fulvestrant led to prolonged therapeutic benefit after
477 treatment cessation in one model, although unlike our model no additional benefit was observed
478 during treatment. The second PDX model responded so effectively to MI-77301 that an additional
479 benefit from combination therapy could not be detected. Our investigations suggest a mechanism
480 of action underlying the combination effect in our models and most probably in prior models.
481 NVP-CGM097 synergised with fulvestrant and the major effect of combination was enhanced
482 downregulation of cell cycle related transcriptional programmes, particularly the E2F regulated
483 transcriptome that when unimpeded is activated as cells progress out of G_1. Our data suggest that
484 combining MDM2 inhibition with endocrine therapy leads to a profound arrest of cell cycle
485 processes and our *in vitro* analysis of the MCF-7 FasR cell line supports this finding, consistent
486 with an increase in senescence as a possible mechanism.
487 CDK4/6 inhibitors in combination with endocrine therapy are the standard of care for advanced
488 breast cancer in the first- and second-line treatment settings. However, resistance to combination
489 therapy will inevitably develop (4), and it is imperative that therapies that can operate in the post
490 resistance setting are identified. We show for the first time that activation of $p53^{wt}$ is effective in
491 a model of CDK4/6 inhibitor-resistant breast cancer. Interestingly, we have demonstrated that p53-
492 induced cell cycle inhibition in palbociclib-resistant MCF-7 is predominantly in the G_2 phase.
493 CDK4/6 inhibition acts to prevent G_1 cell cycle entry by preventing the phosphorylation of Rb
494 (40-42), and many mechanisms of CDK4/6 inhibitor resistance are via disruption of the G_1/S

495 checkpoint (4). Our findings therefore indicate that palbociclib-resistant cell lines that have evaded
496 G_1 checkpoints are still susceptible to G_2 arrest. The combination of MDM2 inhibition and
497 CDK4/6 inhibition engage pathways that remain intact in palbociclib and endocrine resistant cells,
498 unlike the G_1/S checkpoint which is frequently disabled in these resistance contexts.
499 We also show that rechallenging palbociclib-resistant cells with palbociclib in combination with
500 MDM2 inhibition increases B-galactosidase staining and p21 expression, both indicative of
501 senescence. Likewise, fulvestrant-resistant cells treated with combination MDM2 inhibition and
502 fulvestrant become senescent. Senescence entry occurs from either G_1 phase or G_2/M phase (43).
503 Thus, in our models of resistance to either endocrine therapy or palbociclib, NVP-CGM097-
504 mediated induction of G_2/M accumulation along with the downregulation of *FOXM1* and other
505 senescence-related transcripts appears to be sufficient to trigger entry into senescence. CDK4/6
506 inhibitors are known to increase senescence entry and MDM2 can counteract this (44).

507 **Conclusions**

508 Collectively, our results suggest that although ER has been shown to be a negative regulator of
509 p53 (14, 45, 46), it is the anti-proliferative actions of fulvestrant (particularly where they overlap
510 with CDK4/6 inhibition) and MDM2 inhibition interacting via cell cycle progression pathways
511 that combine to produce an enhanced anti-tumour effect. Our data provide a preclinical rationale
512 for the combination of MDM2 inhibition with either endocrine therapy or CDK4/6 inhibition, even
513 in the resistant setting. Importantly, we also offer a novel mechanistic insight that will inform the
514 future design of rational combinations with MDM2 inhibitors in ER-positive breast cancer,
515 demonstrating the efficacy of co-targeting cell cycle pathways and perhaps suggesting an
516 alternative strategy via designing combinations to promote the pro-apoptotic functions of p53.
517

518 **Abbreviations**

519 ER	Estrogen Receptor
520 CDK4/6	Cyclin Dependent Kinase 4 and 6
521 C.I.	Combination Index
522 BrdU	Bromodeoxyuridine
523 P.I.	Propidium Iodide
524 IHC	Immunohistochemistry
525 GSEA	Gene Set Enrichment Analysis
526 GO	Gene Ontology
527 MSigDB	Molecular Signatures Database
528 KEGG	Kyoto Encyclopedia of Genes and Genomes
529 (T)p53wt	p53 (or TP53) wildtype
530 (T)p53mut	p53 (or TP53) mutant
531 IC50	Half maximal Inhibitory Concentration
532 RNASeq	RNA sequencing
533 PDX	Patient Derived Xenograft
534 FasR	Fulvestrant (Faslodex) Resistant
535 PalbR	Palbociclib Resistant

536

537 **Declarations**

538 **Ethics approval and consent to participate:** All *in vivo* experiments, procedures and endpoints
539 were approved by the Garvan Institute of Medical Research Animal Ethics Committee (protocol
540 15/25). PDX models were collected with patient consent under approval from Royal Prince Alfred

541 Hospital human research ethics committee (HREC/13/RPA/187 - KCC_P_3837) and St Vincent's
542 Hospital human research ethics committee (HREC/H2006/2633 - Gar15-13).
543 **Consent for publication:** Not applicable
544 **Availability of data and materials:** The datasets supporting the conclusions of this article are
545 included within the article and its additional files. The read count quantitation and normalized
546 expression matrix for all RNAseq experiments can be downloaded from
547 http://www.ncbi.nlm.nih.gov/geo (GSE140758). Cell lines and PDX models not commercially
548 available can be obtained via MTA with Garvan Institute of Medical Research.
549 **Competing Interests:** Funding and drugs for this study were provided under a research agreement
550 with Novartis Australia.
551 EL provides advisory board services to Novartis Australia, Roche Australia, Specialised
552 Therapeutics Australia, Pfizer Australia, Lilly Australia and Amgen Australia (*All honoraria paid*
553 *to the Garvan Institute of Medical Research*).
554 EH is an employee at Novartis
555 **Funding:** Novartis Australia (NP, HM, EL); National Breast Cancer Foundation (NP: IIRS-19-
556 053, EL: EC17-002 and PRAC14-02); Cancer Institute of New South Wales (HM: ECF171156);
557 Breast Cancer Trials – Australia and New Zealand (EL); The Estate of the late RT Hall (AS); Love
558 Your Sister (EL)
559 **Authors' contributions:** NP, HHM designed and performed experiments, analysed results and
560 wrote the manuscript. EL, CEC analysed results and wrote the manuscript. SA, RC, AY, KJF
561 designed and performed experiments and analysed results. KMC, AS, SH, YH analysed results
562 and provided critical feedback on the manuscript. AP provided critical reagents, oversight of
563 IHC analyses and critical feedback on the manuscript, DS provided critical reagents, EH and
564 WDT provided intellectual input during conception of the project and critical feedback on the
565 manuscript.

566 **Acknowledgements:** Not applicable

567

References

568 1. Lim E, Tarulli G, Portman N, Hickey TE, Tilley WD, Palmieri C. Pushing estrogen receptor around in breast
569 cancer. Endocrine-related cancer. 2016;23(12):T227-T41.
570 2. Hayes EL, Lewis-Wambi JS. Mechanisms of endocrine resistance in breast cancer: an overview of the
571 proposed roles of noncoding RNA. Breast cancer research : BCR. 2015;17:40.
572 3. Turner NC, Slamon DJ, Ro J, Bondarenko I, Im S-A, Masuda N, et al. Overall survival with palbociclib and
573 fulvestrant in advanced breast cancer. New England Journal of Medicine. 2018;379(20):1926-36.
574 4. Portman N, Alexandrou S, Carson E, Wang S, Lim E, Caldon CE. Overcoming CDK4/6 inhibitor resistance
575 in ER positive breast cancer. Endocrine-related cancer. 2018.
576 5. Burgess A, Chia KM, Haupt S, Thomas D, Haupt Y, Lim E. Clinical overview of MDM2/X-targeted
577 therapies. Frontiers in oncology. 2016;6:7.
578 6. Haupt S, Vijayakumaran R, Miranda PJ, Burgess A, Lim E, Haupt Y. The role of MDM2 and MDM4 in
579 breast cancer development and prevention. Journal of molecular cell biology. 2017;9(1):53-61.
580 7. Hock AK, Vousden KH. The role of ubiquitin modification in the regulation of p53. Biochimica et biophysica
581 acta. 2014;1843(1):137-49.
582 8. Haupt Y, Maya R, Kazaz A, Oren M. Mdm2 promotes the rapid degradation of p53. Nature.
583 1997;387(6630):296-9.
584 9. Kubbutat MH, Jones SN, Vousden KH. Regulation of p53 stability by Mdm2. Nature. 1997;387(6630):299-
585 303.
586 10. Li M, Brooks CL, Wu-Baer F, Chen D, Baer R, Gu W. Mono- versus polyubiquitination: differential control
587 of p53 fate by Mdm2. Science. 2003;302(5652):1972-5.
588 11. Yu Q, Li Y, Mu K, Li Z, Meng Q, Wu X, et al. Amplification of Mdmx and overexpression of MDM2
589 contribute to mammary carcinogenesis by substituting for p53 mutations. Diagnostic pathology. 2014;9:71.
590 12. Swetzig WM, Wang J, Das GM. Estrogen receptor alpha (ERα/ESR1) mediates the p53-independent
591 overexpression of MDM4/MDMX and MDM2 in human breast cancer. Oncotarget. 2016;7(13):16049.
592 13. Dolfi SC, Jäger AV, Medina DJ, Haffty BG, Yang J-M, Hirshfield KM. Fulvestrant treatment alters MDM2
593 protein turnover and sensitivity of human breast carcinoma cells to chemotherapeutic drugs. Cancer letters.
594 2014;350(1-2):52-60.
595 14. Bailey ST, Shin H, Westerling T, Liu XS, Brown M. Estrogen receptor prevents p53-dependent apoptosis in
596 breast cancer. Proceedings of the National Academy of Sciences. 2012;109(44):18060-5.
597 15. Caldon CE. Estrogen signaling and the DNA damage response in hormone dependent breast cancers.
598 Frontiers in oncology. 2014;4:106.
599 16. Lu J, McEachern D, Li S, Ellis MJ, Wang S. Reactivation of p53 by mdm2 inhibitor mi-77301 for the
600 treatment of endocrine-resistant breast cancer. Molecular cancer therapeutics. 2016;15(12):2887-93.
601 17. Holzer P, Masuya K, Furet P, Kallen J, Valat-Stachyra T, Ferretti Sp, et al. Discovery of a
602 dihydroisoquinolinone derivative (NVP-CGM097): a highly potent and selective MDM2 inhibitor undergoing phase
603 1 clinical trials in p53wt tumors. ACS Publications; 2015.
604 18. Bauer S, Demetri G, Jeay S, Dummer R, Guerreiro N, Tan DS, et al. 366PD - A phase I, open-label, multi-
605 center, dose escalation study of oral NVP-CGM097, a p53/HDM2-protein-protein interaction inhibitor, in adult
606 patients with selected advanced solid tumors,. Annals of Oncology. 2016;27(S6):vi116.
607 19. Chou TC, Talalay P. Quantitative analysis of dose-effect relationships: the combined effects of multiple drugs
608 or enzyme inhibitors. Advances in enzyme regulation. 1984;22:27-55.
609 20. Chia K, Milioli H, Portman N, Laven-Law G, Coulson R, Yong A, et al. Non-canonical AR activity facilitates
610 endocrine resistance in breast cancer. Endocrine-related cancer. 2019;26(2):251-64.
611 21. Oakes SR, Vaillant F, Lim E, Lee L, Breslin K, Feleppa F, et al. Sensitization of BCL-2–expressing breast
612 tumors to chemotherapy by the BH3 mimetic ABT-737. Proceedings of the National Academy of Sciences.
613 2012;109(8):2766-71.
614 22. Liao Y, Smyth GK, Shi W. featureCounts: an efficient general purpose program for assigning sequence reads
615 to genomic features. Bioinformatics. 2013;30(7):923-30.
616 23. Robinson MD, McCarthy DJ, Smyth GK. edgeR: a Bioconductor package for differential expression analysis
617 of digital gene expression data. Bioinformatics. 2010;26(1):139-40.

618 24. McCarthy DJ, Chen Y, Smyth GK. Differential expression analysis of multifactor RNA-Seq experiments
619 with respect to biological variation. Nucleic acids research. 2012;40(10):4288-97.
620 25. Ritchie ME, Phipson B, Wu D, Hu Y, Law CW, Shi W, et al. limma powers differential expression analyses
621 for RNA-sequencing and microarray studies. Nucleic acids research. 2015;43(7):e47-e.
622 26. Yu G, Wang L-G, Han Y, He Q-Y. clusterProfiler: an R package for comparing biological themes among
623 gene clusters. Omics: a journal of integrative biology. 2012;16(5):284-7.
624 27. Reuther C, Heinzle V, Nolting S, Herterich S, Hahner S, Halilovic E, et al. The HDM2 (MDM2) Inhibitor
625 NVP-CGM097 Inhibits Tumor Cell Proliferation and Shows Additive Effects with 5-Fluorouracil on the p53-p21-Rb-
626 E2F1 Cascade in the p53wild type Neuroendocrine Tumor Cell Line GOT1. Neuroendocrinology. 2018;106(1):1-19.
627 28. Weisberg E, Halilovic E, Cooke VG, Nonami A, Ren T, Sanda T, et al. Inhibition of Wild-Type p53-
628 Expressing AML by the Novel Small Molecule HDM2 Inhibitor CGM097. Mol Cancer Ther. 2015;14(10):2249-59.
629 29. Holzer P, Masuya K, Furet P, Kallen J, Valat-Stachyra T, Ferretti S, et al. Discovery of a
630 Dihydroisoquinolinone Derivative (NVP-CGM097): A Highly Potent and Selective MDM2 Inhibitor Undergoing
631 Phase 1 Clinical Trials in p53wt Tumors. Journal of medicinal chemistry. 2015;58(16):6348-58.
632 30. Tao YF, Wang NN, Xu LX, Li ZH, Li XL, Xu YY, et al. Molecular mechanism of G1 arrest and cellular
633 senescence induced by LEE011, a novel CDK4/CDK6 inhibitor, in leukemia cells. Cancer cell international.
634 2017;17:35.
635 31. Xie Q, Wu Q, Mack SC, Yang K, Kim L, Hubert CG, et al. CDC20 maintains tumor initiating cells.
636 Oncotarget. 2015;6(15):13241-54.
637 32. Laoukili J, Kooistra MR, Bras A, Kauw J, Kerkhoven RM, Morrison A, et al. FoxM1 is required for execution
638 of the mitotic programme and chromosome stability. Nature cell biology. 2005;7(2):126-36.
639 33. Vilgelm AE, Saleh N, Shattuck-Brandt R, Riemenschneider K, Slesur L, Chen SC, et al. MDM2 antagonists
640 overcome intrinsic resistance to CDK4/6 inhibition by inducing p21. Science translational medicine. 2019;11(505).
641 34. Patnaik A, Rosen LS, Tolaney SM, Tolcher AW, Goldman JW, Gandhi L, et al. Efficacy and Safety of
642 Abemaciclib, an Inhibitor of CDK4 and CDK6, for Patients with Breast Cancer, Non-Small Cell Lung Cancer, and
643 Other Solid Tumors. Cancer discovery. 2016;6(7):740-53.
644 35. Tisato V, Voltan R, Gonelli A, Secchiero P, Zauli G. MDM2/X inhibitors under clinical evaluation:
645 perspectives for the management of hematological malignancies and pediatric cancer. J Hematol Oncol.
646 2017;10(1):133.
647 36. Nair AB, Jacob S. A simple practice guide for dose conversion between animals and human. J Basic Clin
648 Pharm. 2016;7(2):27-31.
649 37. Spring LM, Wander SA, Andre F, Moy B, Turner NC, Bardia A. Cyclin-dependent kinase 4 and 6 inhibitors
650 for hormone receptor-positive breast cancer: past, present, and future. Lancet. 2020;395(10226):817-27.
651 38. Jeay S, Ferretti S, Holzer P, Fuchs J, Chapeau EA, Wartmann M, et al. Dose and Schedule Determine Distinct
652 Molecular Mechanisms Underlying the Efficacy of the p53-MDM2 Inhibitor HDM201. Cancer research.
653 2018;78(21):6257-67.
654 39. Fischer M, Quaas M, Steiner L, Engeland K. The p53-p21-DREAM-CDE/CHR pathway regulates G2/M cell
655 cycle genes. Nucleic Acids Res. 2016;44(1):164-74.
656 40. Petrossian K, Kanaya N, Lo C, Hsu PY, Nguyen D, Yang L, et al. ERalpha-mediated cell cycle progression
657 is an important requisite for CDK4/6 inhibitor response in HR+ breast cancer. Oncotarget. 2018;9(45):27736-51.
658 41. Prall OW, Rogan EM, Sutherland RL. Estrogen regulation of cell cycle progression in breast cancer cells.
659 The Journal of steroid biochemistry and molecular biology. 1998;65(1-6):169-74.
660 42. Foster JS, Wimalasena J. Estrogen regulates activity of cyclin-dependent kinases and retinoblastoma protein
661 phosphorylation in breast cancer cells. Molecular endocrinology. 1996;10(5):488-98.
662 43. Sharpless NE, Sherr CJ. Forging a signature of in vivo senescence. Nature reviews Cancer. 2015;15(7):397-
663 408.
664 44. Klein ME, Dickson MA, Antonescu C, Qin LX, Dooley SJ, Barlas A, et al. PDLIM7 and CDH18 regulate
665 the turnover of MDM2 during CDK4/6 inhibitor therapy-induced senescence. Oncogene. 2018;37(37):5066-78.
666 45. Konduri SD, Medisetty R, Liu W, Kaipparettu BA, Srivastava P, Brauch H, et al. Mechanisms of estrogen
667 receptor antagonism toward p53 and its implications in breast cancer therapeutic response and stem cell regulation.
668 Proceedings of the National Academy of Sciences of the United States of America. 2010;107(34):15081-6.
669 46. Sayeed A, Konduri SD, Liu W, Bansal S, Li F, Das GM. Estrogen receptor alpha inhibits p53-mediated
670 transcriptional repression: implications for the regulation of apoptosis. Cancer research. 2007;67(16):7746-55.

671

672 **Figure Legends**

673 **Fig 1. MDM2 inhibition reduces viability in a p53 dependent manner in cell line models of**

674 **ER+ breast cancer.**

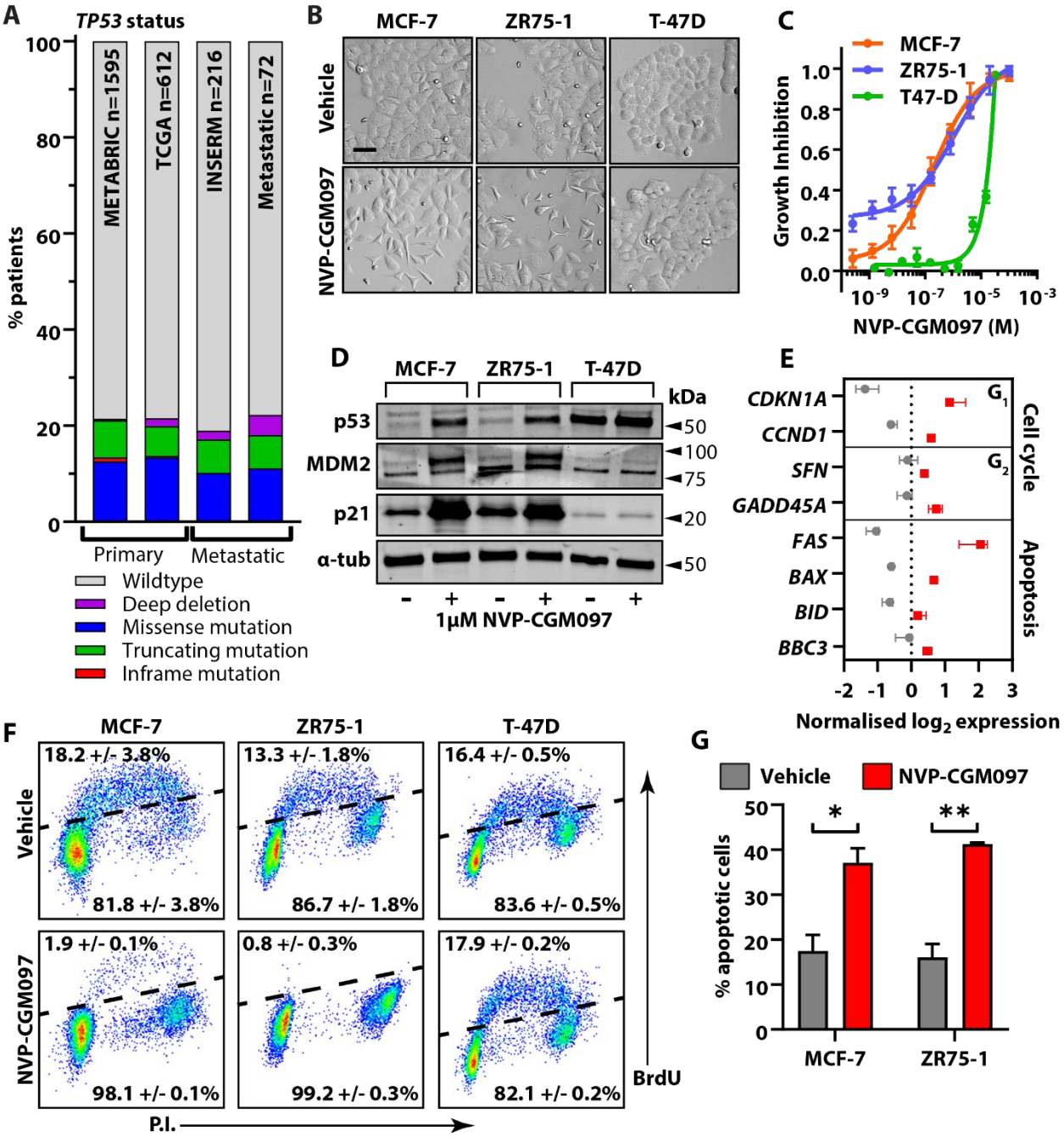

675

676 **A.** The frequency of p53 mutation (putative drivers) in ER-positive primary breast cancers – Breast

677 Cancer (METABRIC, Nature 2012 & Nat Commun 2016), Breast Invasive Carcinoma (TCGA,

678 Cell 2015) – and metastatic tumours – The Metastatic Breast Cancer Project (Provisional, October

679 2018) and Metastatic Breast Cancer (INSERM, PLoS Med 2016) – across public datasets in
680 https://www.cbioportal.org/. **B.** Representative images of MCF-7, ZR75-1 and T-47D cell cultures
681 after exposure to vehicle (0.01% DMSO) or 1μM NVP-CGM097 for 48 hours. Bar = 20μm. **C.**
682 Growth inhibition relative to vehicle after 48 hours treatment with escalating doses of NVP-
683 CGM097 in $p53^{wt}$ MCF-7 (orange) and ZR75-1 (blue), and $p53^{mut}$ T-47D cells (green). **D.** Western
684 blot analysis of p53 and the known p53 transcriptional targets MDM2 and p21 after 48 hours
685 incubation with 1μM NVP-CGM097. α-tubulin staining is shown as an indication of relative
686 loading. See Fig. S1A for full gel and blot images. **E.** Normalised expression of cell cycle
687 regulators and apoptosis markers after treatment with vehicle (0.01% DMSO, grey) or 1μM NVP-
688 CGM097 (red) for 48 hours in MCF-7 cell lines. **F.** Flow cytometry analysis of the incorporation
689 of BrdU over a 2-hour period in MCF-7, ZR75-1 and T-47D following a 48 hour incubation with
690 1μM NVP-CGM097. **G.** Proportion of MCF-7 and ZR75-1 cells staining positive for AnnexinV
691 after treatment for 48 hours with vehicle (grey) or 1μM NVP-CGM097 (red). Statistical
692 significance from Tukey's multiple comparison test is indicated above each column.
693

694 **Fig 2. MDM2 inhibition reduces tumour growth and proliferation markers in an ER+**

695 **breast cancer PDX model.**

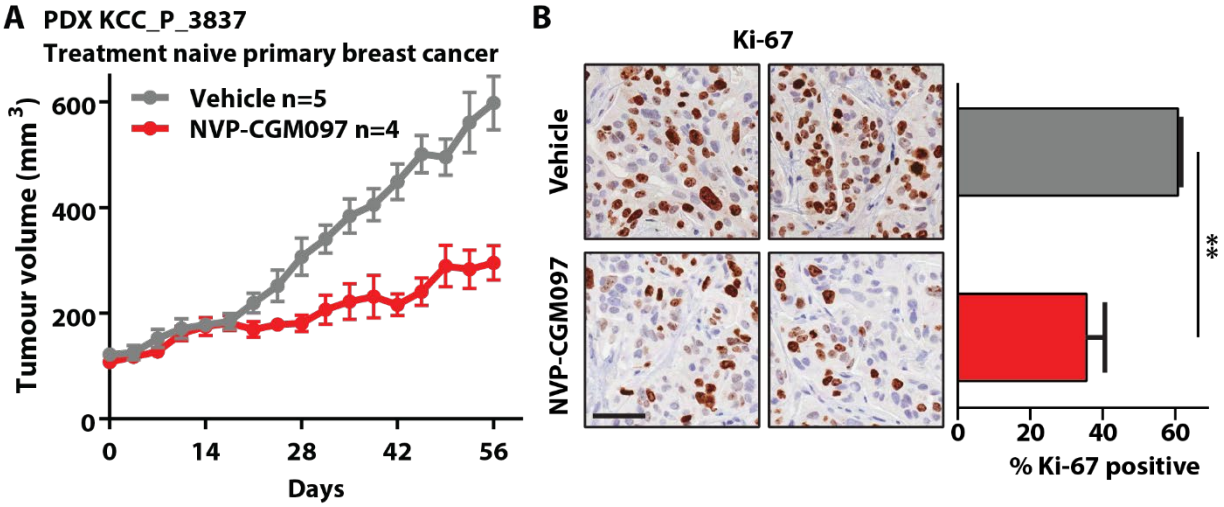

696

697 **A.** Growth of the treatment naïve KCC_P_3837 PDX model of ER+ breast cancer treated with

698 vehicle (2% DMSO daily, grey, n=5) and NVP-CGM097 (100mg/kg daily, red, n=4) for 60 days.

699 **B.** Representative images and quantification of the proliferation marker Ki-67 at endpoint. Ki-67

700 positive proportions from three independent replicates per treatment were compared by two-

701 tailed T test. Bar = 50µm.

702

703 **Fig 3. MDM2 inhibition and endocrine therapy synergistically reduce proliferation and**

704 **downregulate hallmark gene sets of cell cycle progression.**

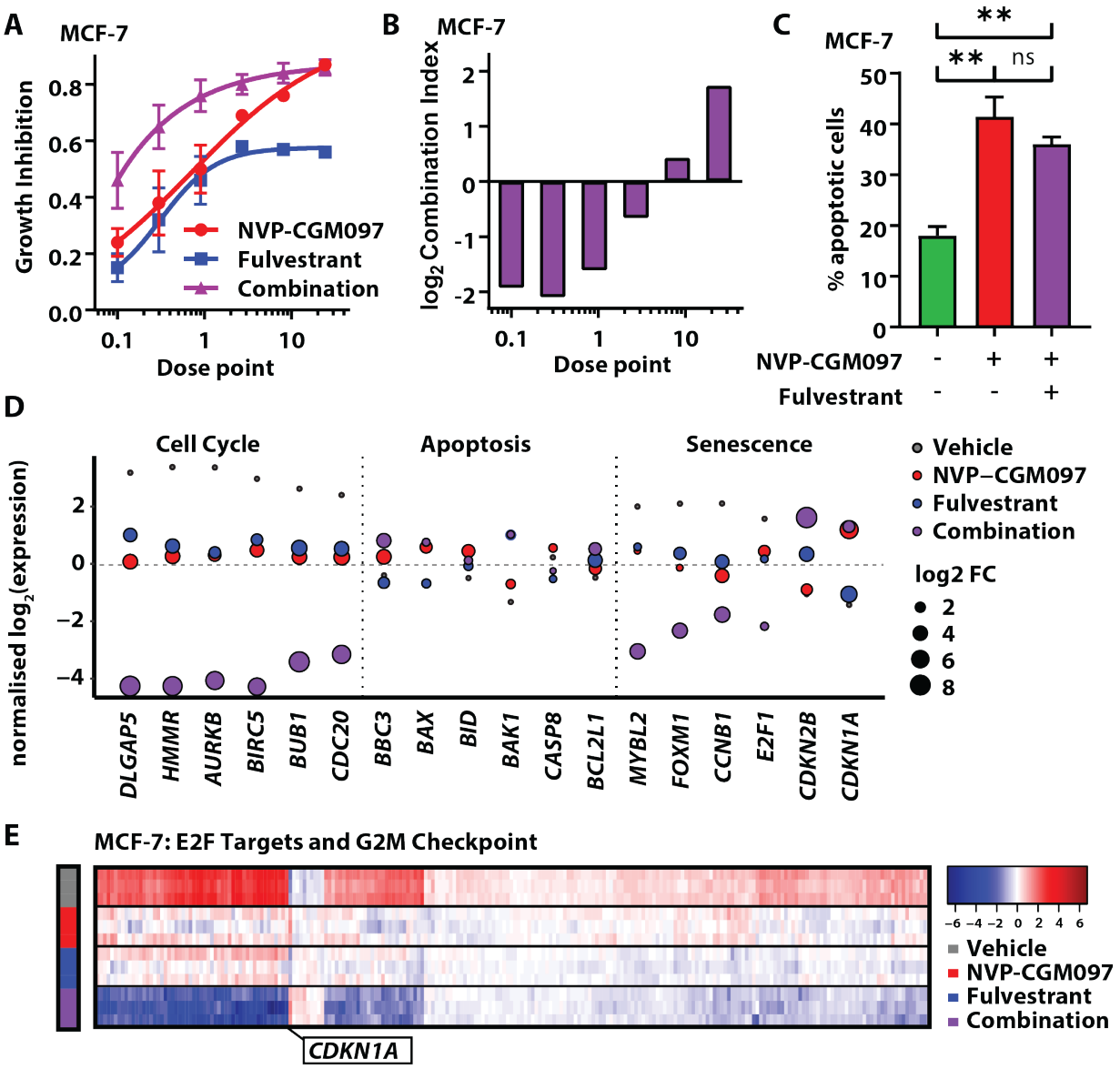

705

706 **A.** Growth inhibition relative to vehicle of escalating doses of NVP-CGM097 (red) and fulvestrant

707 (blue) alone and in combination (purple) **B.** $\log_2$ (combination index) calculated from results in **A.**

708 Values below 0 (equivalent to combination index < 1) indicate synergy. Dose points: NVP-

709 CGM097 x100nM; fulvestrant x0.1nM. **C.** Proportion of MCF-7 cells staining positive for

710 Annexin V (apoptotic cells) after treatment for 48 hours with vehicle (green), 1μM NVP-CGM097

711 (red), or the combination of 1μM NVP-CGM097 and 1nM fulvestrant (purple). Statistical

712 significance from Tukey's multiple comparison test is indicated above each column. **D.**

713 Normalised log2 expression of significant p53 target genes induced by treatment for 48 hours with
714 NVP-CGM097 (1μM, red), fulvestrant (1nM, blue) and combination (1μM NVP-CGM097 and
715 1nM fulvestrant, purple), averaged by condition, associated with cell cycle, apoptosis and
716 senescence. **E.** Heat map of significant downregulated genes from the E2F Targets and G_2/M
717 Checkpoint Molecular Signatures Database (MSigDB) gene sets, normalised by gene (row), in
718 MCF-7 cell lines for each condition: vehicle (0.01% DMSO), NVP-CGM097 (1μM), fulvestrant
719 (1nM) and combination (1μM NVP-CGM097 and 1nM fulvestrant).
720

721 **Fig 4. Fulvestrant potentiates MDM2 inhibition in a fulvestrant resistant cell line model.**

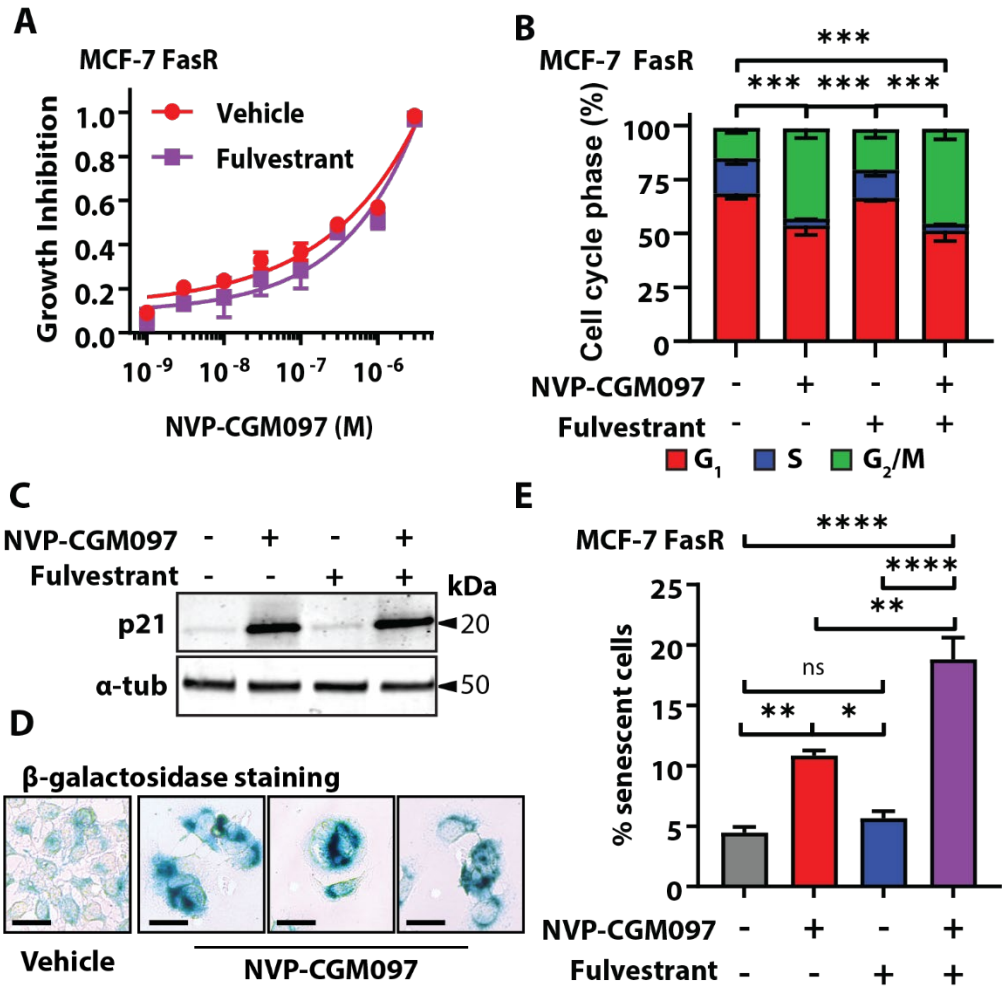

722

723 **A.** Growth inhibition of MCF-7 FasR relative to vehicle with escalating doses of NVP-CGM097
724 in the presence (purple) or absence (red) of 100nM fulvestrant – the dose used to generate the
725 resistant cell line. No significant difference was observed after 48 hours of treatment. **B.** Flow
726 cytometric quantification of propidium iodide incorporation into DNA compared to vehicle in
727 MCF-7 FasR after incubation for 48 hours with vehicle (0.01% DMSO), 1μM NVP-CGM097,
728 100nM fulvestrant, or the combination of both drugs. Statistical significance from χ^2 test using the
729 vehicle treated profile as the expected value is indicated. Red = G_1 (bottom), blue = S (middle),
730 green = G_2/M (top). **C.** Western blot analysis of the p53 transcriptional target p21 in MCF-7 FasR
731 cells after 48 hours incubation with 1μM NVP-CGM097. α-tubulin staining is shown as an
732 indication of relative loading. See Fig. S4B for full gel and blot images. **D.** Representative images

733 of MCF-7 FasR cell cultures after exposure to vehicle (0.01% DMSO) or 1μM NVP-CGM097 for
734 48 hours followed by staining for senescence associated β-galactosidase. Bar = 20 μm **E.**
735 Quantification of MCF-7 FasR cells staining positive for senescence associated β-galactosidase
736 activity after treatment for 48 hours with vehicle (0.01% DMSO, grey), 1μM NVP-CGM097 (red),
737 100nM fulvestrant (blue), or the combination of NVP-CGM097 and fulvestrant (purple). Statistical
738 significance from Tukey's multiple comparison test is indicated above each column.
739

740 **Fig 5. Fulvestrant potentiates MDM2 inhibition *in vivo* in a PDX model of fulvestrant**

741 **resistant ER+ breast cancer.**

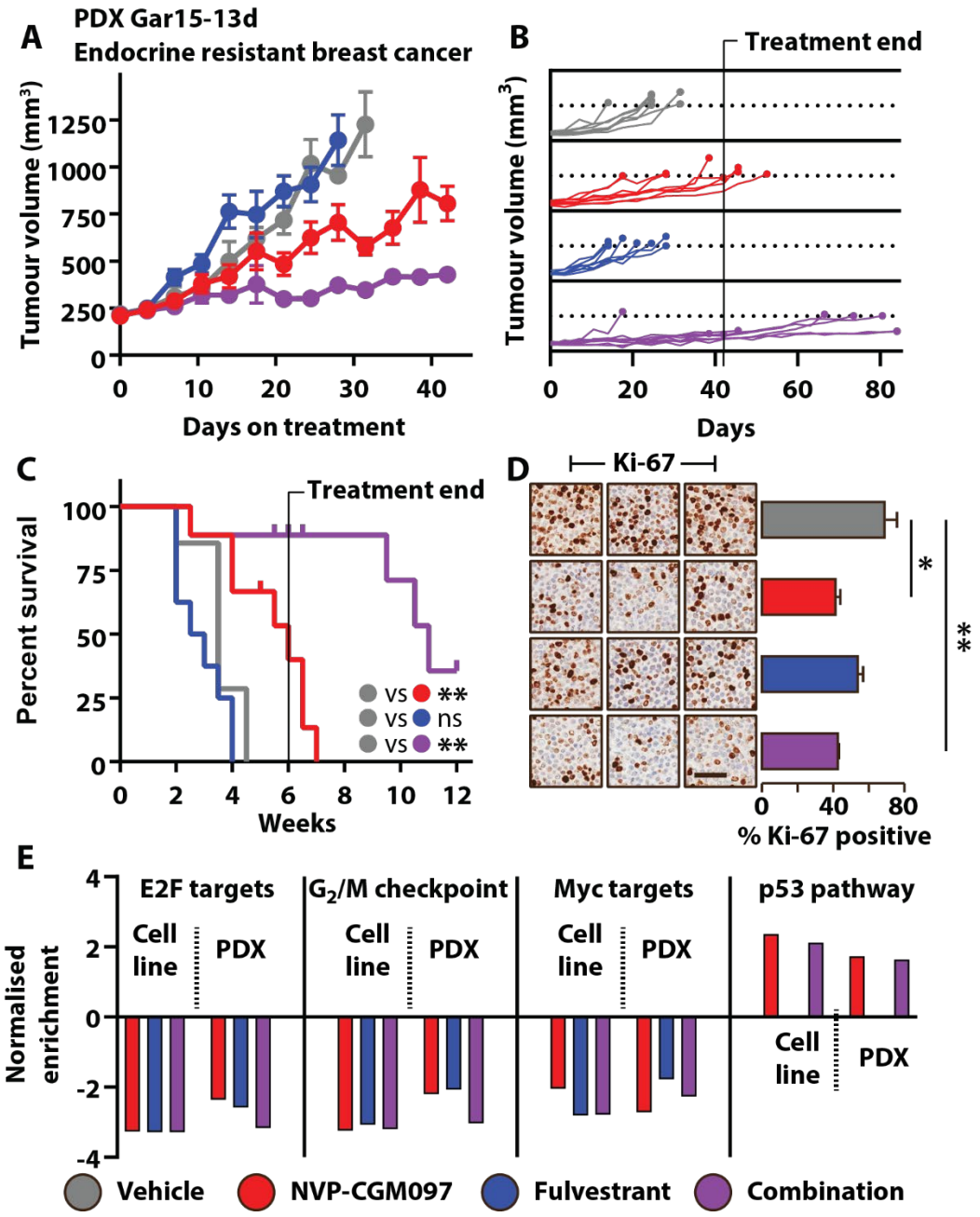

742

743 **A.** Growth of the endocrine resistant Gar15-13 PDX model of ER+ breast cancer treated with

744 vehicle (2% DMSO daily, grey, n=7), NVP-CGM097 (100mg/kg daily, red, n=8), fulvestrant

745 (5mg/body weekly, blue, n=8) or the combination of NVP-CGM097 and fulvestrant (purple, n=9).

746 **B.** Continued growth of tumours following withdrawal of treatment after 6 weeks. **C.** Survival

747 analysis of outcomes after treatment with combination therapy compared to each drug alone (an

748 event was defined as a tumour exceeding 999 mm^3). Curves were compared using Mantel-Cox
749 log-rank test and significance is indicated for comparisons of each arm with vehicle. **D.**
750 Representative images and quantification of IHC staining for Ki-67 of three independent replicates
751 per treatment arm from tumours treated for 10 days. Statistical significance from Tukey's multiple
752 comparison test is indicated. Bar = 50µm. **E.** GSEA analysis compared to vehicle performed across
753 gene expression sets of *in vitro* and *in vivo* models following treatment with NVP-CGM097 (red),
754 fulvestrant and combination therapy show consistent regulation of hallmark signatures from
755 MSigDB: E2F Targets, G_2/M Checkpoints, MYC Targets and p53 Pathway. This analysis is
756 reinforced by the normalized enrichment score (NES) that shows the difference in gene set size
757 following each treatment conditions.
758

759 **Figure 6. MDM2 inhibition synergises with palbociclib to reduce proliferation via cell cycle**

760 **arrest.**

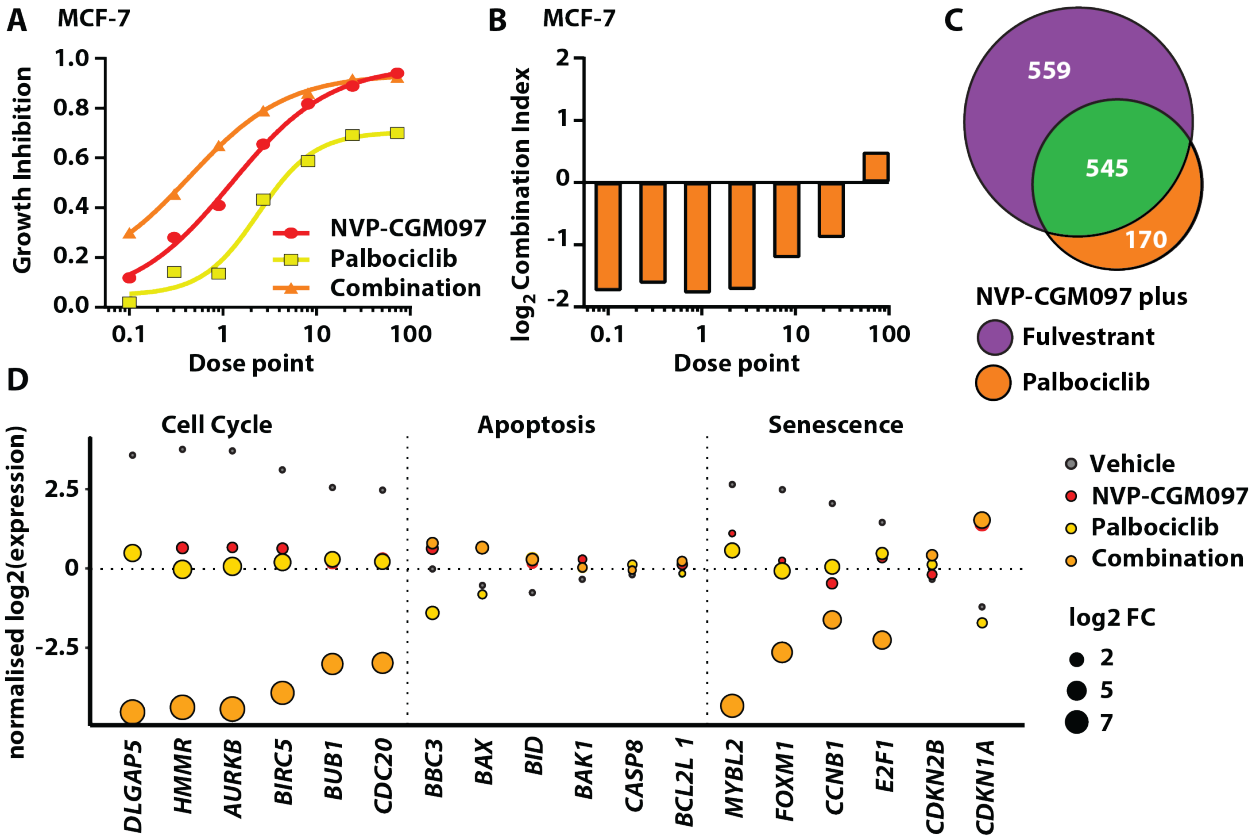

761

762 **A.** Growth inhibition relative to vehicle of escalating doses of NVP-CGM097 (red) and palbociclib

763 (yellow) alone and in combination (orange) **B.** $\log_2$ (combination index) calculated from results in

764 **A.** Values below 0 (equivalent to combination index < 1) indicate synergy. Dose points: NVP-

765 CGM097 x100nM; palbociclib x50nM. **C.** Venn diagram showing the overlap (green) between

766 differentially expressed genes (adjusted p-value < 0.05- and 2-fold change) induced in MCF-7

767 cells by treatment for 48 hours with combination therapies, 1μM NVP-CGM097 plus 1nM

768 fulvestrant (purple) and 1μM NVP-CGM097 plus 500nM palbociclib (orange). **D.** Normalised $\log_2$

769 expression levels of significant p53 target genes induced by treatment with NVP-CGM097 (1μM);

770 palbociclib (500nM) and combination (1μM NVP-CGM097 and 500nM palbociclib), averaged by

771 condition, associated with cell cycle, apoptosis and senescence.

772 **Figure 7. Palbociclib potentiates MDM2 inhibition via an increase in senescence in**

773 **palbociclib resistant MCF-7.**

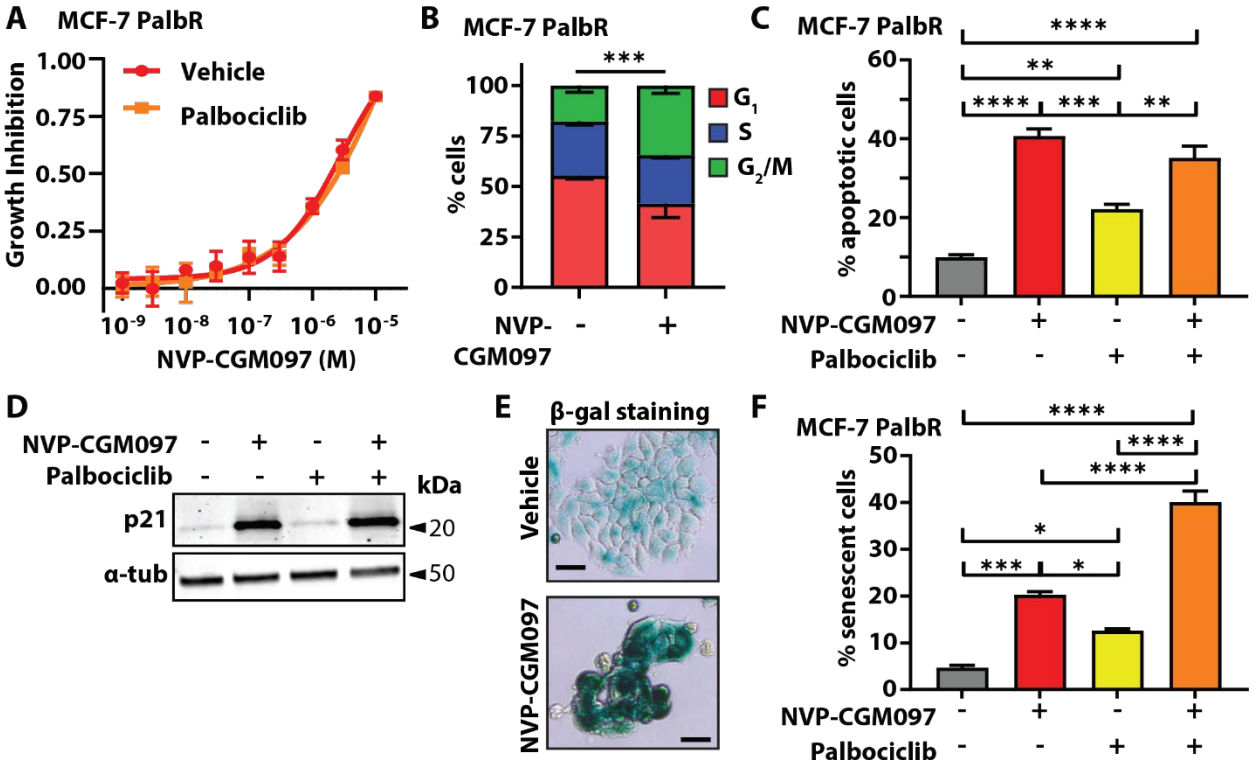

774

775 **A.** Growth inhibition of MCF-7 PalbR relative to vehicle (0.01% DMSO) of escalating doses of

776 NVP-CGM097 in the presence (red) or absence (yellow) of 500nM palbociclib – the dose used to

777 generate the resistant cell line. No significant difference was observed after 48 hours of treatment.

778 **B.** Proportion of cells in each cell cycle phase from flow cytometric quantification of propidium

779 iodide staining of genomic DNA in MCF-7 PalbR cells after 48 hours treatment with 1μM NVP-

780 CGM097 compared to vehicle (500nM palbociclib, 0.01% DMSO). Statistical significance from

781 χ^2 test using the vehicle treated profile as the expected value is indicated. Red = G_1 (bottom), blue

782 = S (middle), green = G_2/M (top). **C.** Proportion of MCF-7 PalbR cells staining positive for

783 AnnexinV after treatment for 48 hours with vehicle (0.01% DMSO, grey), 1μM NVP-CGM097

784 (red), 500nM palbociclib (yellow) or the combination of 1μM NVP-CGM097 and 500nM

785 palbociclib (orange). Statistical significance from Tukey's multiple comparison test is indicated

786 above each column. **D.** Western blot analysis of p21 in MCF-7 PalbR cells after 48 hours

787 incubation with 1μM NVP-CGM097. α-tubulin staining is shown as an indication of relative
788 loading. See Fig. S5D for full gel and blot images. **E.** Representative images of MCF-7 PalbR cell
789 cultures after exposure to vehicle (500nM palbociclib, 0.01% DMSO) or 1μM NVP-CGM097 for
790 48 hours followed by staining for senescence associated β-galactosidase. Bar = 20μm **F.**
791 Quantification of MCF-7 PalbR cells staining positive for senescence associated β-galactosidase
792 activity after treatment for 48 hours with vehicle (0.01% DMSO, grey), 1μM NVP-CGM097 (red),
793 500nM palbociclib (yellow), or the combination of NVP-CGM097 and palbociclib (orange).
794 Statistical significance from Tukey's multiple comparison test is indicated above each column.
795

796 **Supplementary materials**

797

798 **Table S1:** Differential expression analysis of MCF7 cell lines following 48 hours treatment with
799 NVP-CGM097 versus vehicle (0.01% DMSO).

800 **Table S2:** Differential expression analysis of MCF7 cell lines following 48 hours treatment with
801 Fulvestrant versus vehicle (0.01% DMSO).

802 **Table S3:** Differential expression analysis of MCF7 cell lines following 48 hours treatment with
803 combination therapy (NVP-CGM097 + fulvestrant) versus vehicle (0.01% DMSO).

804 **Table S4:** Differential genes induced by combination therapy (NVP-CGM097 + fulvestrant)
805 versus vehicle (0.01% DMSO).

806 **Table S5:** KEGG PATHWAY enrichment analysis of differentially expressed genes following
807 treatment with combination of NVP-CGM097 and fulvestrant versus vehicle (0.01% DMSO).

808 **Table S6:** Combination effect quantified for all genes following treatment with NVP-CGM097,
809 fulvestrant and combination across cell lines.

810 **Table S7:** Differential expression analysis of the PDX breast cancer model treated with NVP-
811 CGM097 versus vehicle.

812 **Table S8:** Differential expression analysis of the PDX breast cancer model treated with fulvestrant
813 versus vehicle.

814 **Table S9:** Differential expression analysis of the PDX breast cancer model treated with
815 combination therapy versus vehicle.

816 **Table S10.** Gene set enrichment analysis of DE genes induced by NVP-CGM097 in MCF-7 cell
817 lines.

818 **Table S11.** Gene set enrichment analysis of DE genes induced by fulvestrant in MCF-7 cell lines.

819 **Table S12.** Gene set enrichment analysis of DE genes induced by combination therapy in MCF-7
820 cell lines.

821 **Table S13.** Gene set enrichment analysis of DE genes induced by NVP-CGM097 in the PDX
822 treated model.
823 **Table S14.** Gene set enrichment analysis of DE genes induced by fulvestrant in the PDX treated
824 model.
825 **Table S15.** Gene set enrichment analysis of DE genes induced by combination therapy in the PDX
826 treated model.
827 **Table S16:** Combination effect quantified for all genes following treatment with NVP-CGM097,
828 fulvestrant and combination in the PDX model.
829 **Table S17**: Differential expression analysis of MCF7 cell lines following 48 hours treatment with
830 NVP-CGM097 versus vehicle (0.01% DMSO).
831 **Table S18:** Differential expression analysis of MCF7 cell lines following 48 hours treatment with
832 palbociclib versus vehicle (0.01% DMSO).
833 **Table S19:** Differential expression analysis of MCF7 cell lines following 48 hours treatment with
834 combination therapy (NVP-CGM097 + palbociclib) versus vehicle (0.01% DMSO).
835 **Table S20:** Combination effect quantified for all genes following treatment with NVP-CGM097,
836 palbociclib and combination across cell lines.

Fig. S1. MDM2 inhibition activates p53 and reduces tumour proliferation *in vitro* and *in vivo*.

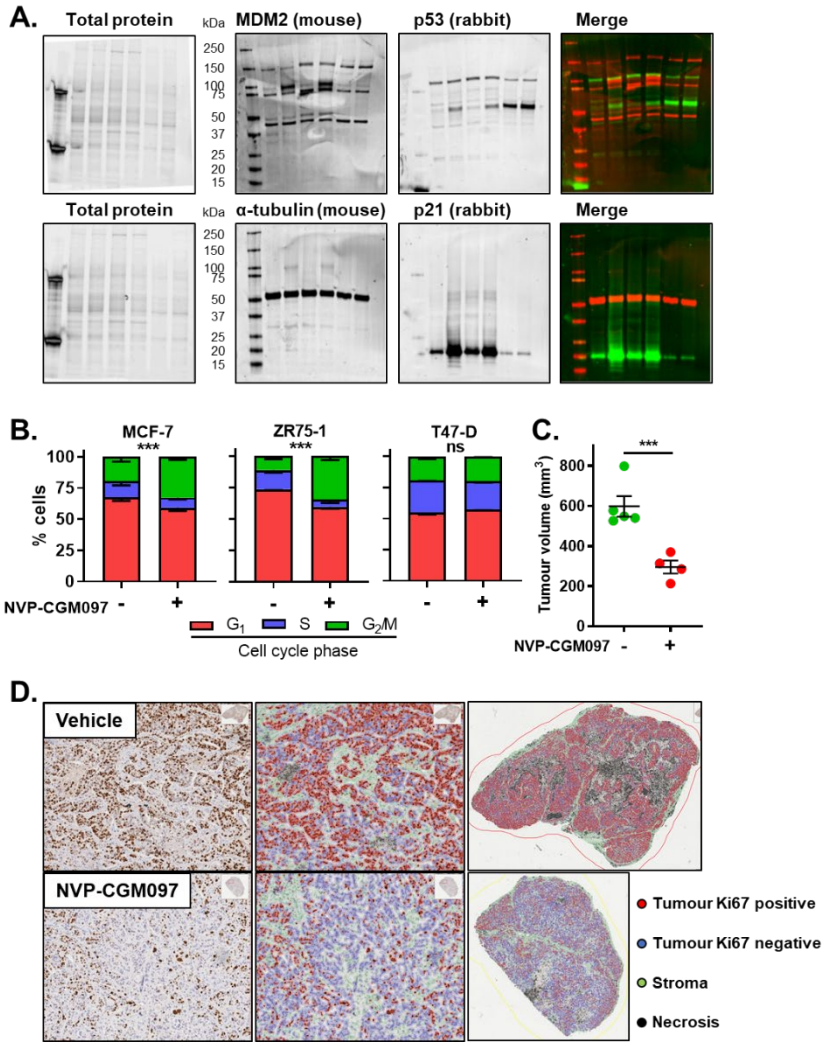

A. Full gel and blot scans for the Western blots shown in Fig. 1B. Total protein was visualised using BioRad stain-free imaging technology according to the manufacturer's instructions. **B.** Analysis of cell cycle phase using flow cytometry to quantify propidium iodide staining of genomic DNA shows significant alterations to cell cycle phase distribution in $p53^{wt}$ models consistent with arrest in both G_1 and G_2 after incubation for 48 hours with 1μM NVP-CGM097. Red = G_1 (bottom), blue = S (middle), green = G_2/M (top). Statistical significance from χ^2 test using the vehicle treated profile as the expected value is indicated. **C.** NVP-CGM097 (50mg/kg daily, red) significantly inhibited tumour volumes compared to vehicle (2% DMSO daily, green) at endpoint. Final tumour volumes were compared using two-tailed T test to determine significance. **D.** Representative images of Ki-67 quantification of endpoint tumours in Qupath software showing the classification of different tissue compartments: tumour (red and blue), stroma (green), and necrosis (black); and detection of Ki-67 negative and positive tumour cells. A single classifier was applied to all tumour sections.

Fig. S2. NVP-CGM097 treatment causes gene expression changes in cell cycle and p53 pathways *in vitro*.

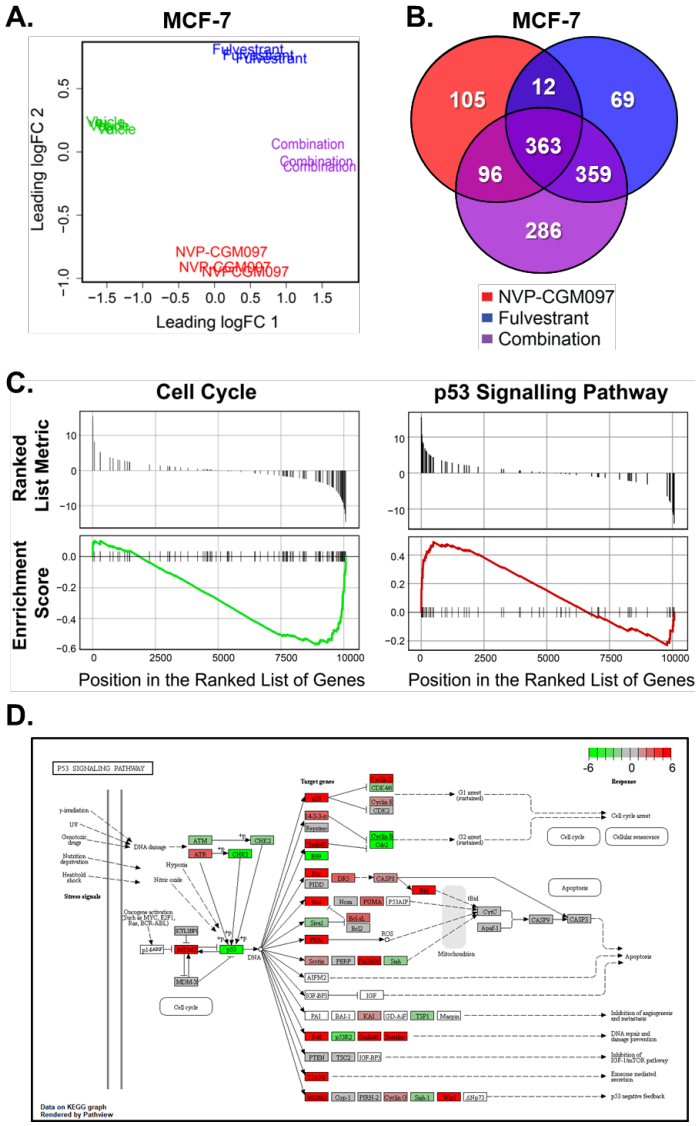

A. Multidimensional scaling (MDS) plot showing the level of sample similarity between MCF-7 cell lines treated with vehicle, NVP-CGM097, fulvestrant and combination therapy (NVP-CGM097 plus fulvestrant). **B.** Venn diagram showing the overlap between differentially expressed genes (adjusted p-value < 0.05- and 2-fold change) induced by treatment in MCF-7 cell lines. **C.** KEGG pathway analysis using RNA-Seq transcriptomic data shows a significant negative enrichment of Cell Cycle regulation in MCF-7 cell lines following 48 hours of treatment with 1µM NVP-CGM097 and positive enrichment of p53 Signalling Pathway. **D.** KEGG enrichment analysis showing p53 Signalling Pathway activation in MCF-7 cell lines following treatment with NVP-CGM097.

Fig. S3. Enrichment analysis of significant differentially expressed genes against curated gene sets.

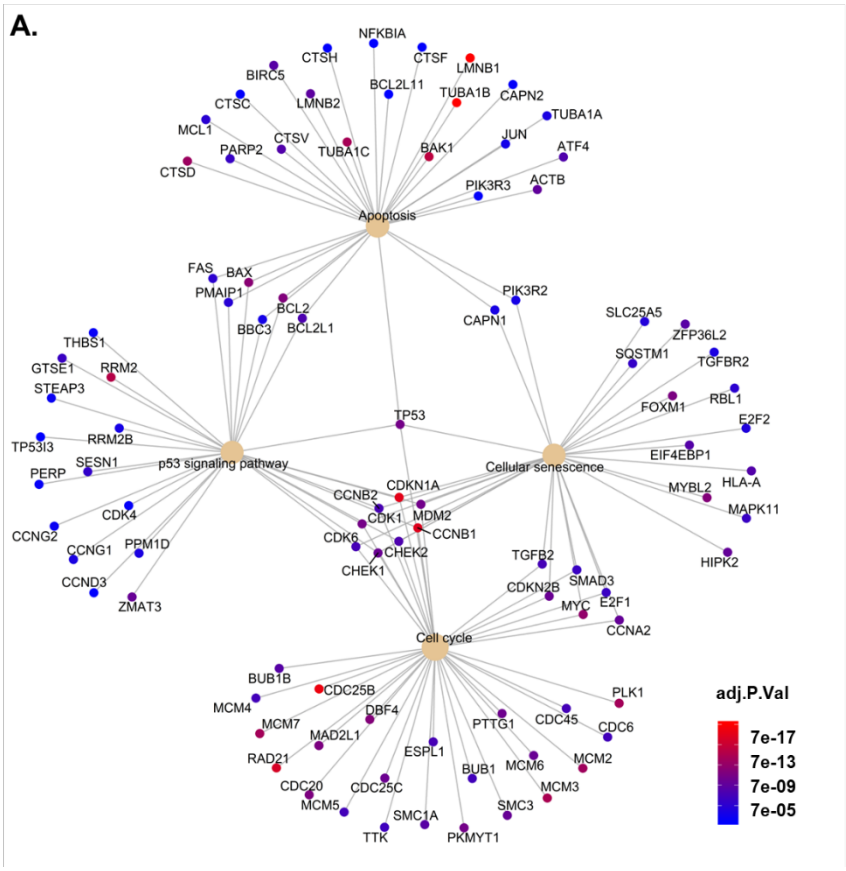

Fig. S4. MDM2 inhibition induces changes in gene and protein expression associated with the cell cycle in endocrine resistant models *in vitro* and *in vivo*.

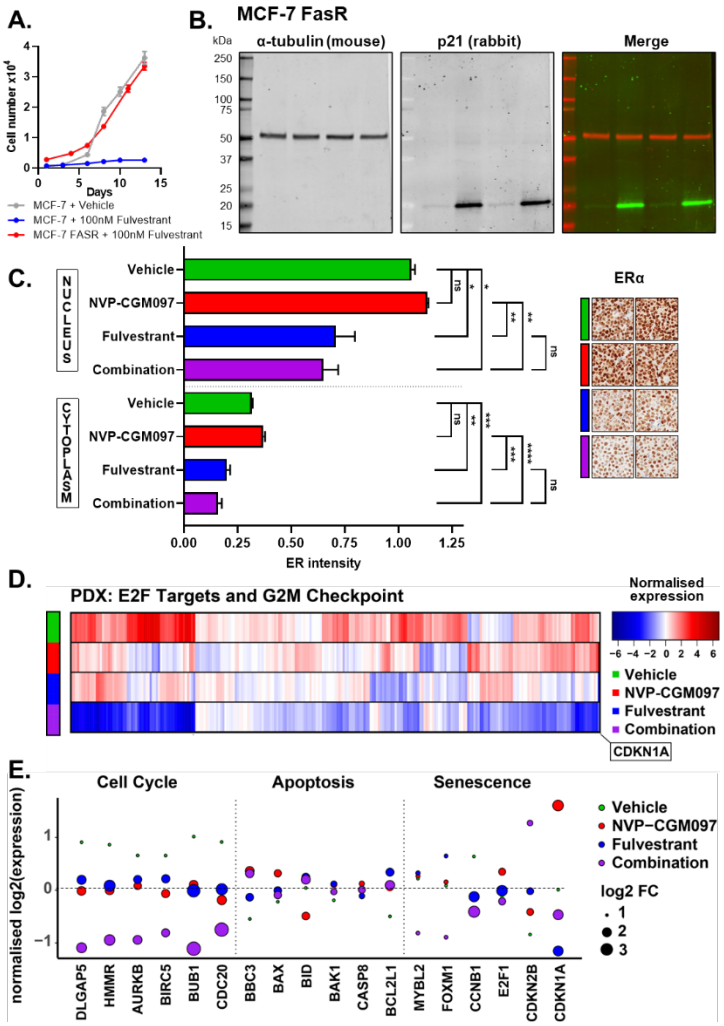

A. Incucyte analysis of cell numbers of parental MCF-7 cells (blue) and MCF-7 FasR cells (red) over time after treatment with 100nM fulvestrant. Vehicle treated parental MCF-7 cell growth (grey) is shown for comparison. **B.** Full gel images for the Western blots shown in Fig. 4C. **C.** Quantification of ER staining in the nucleus and cytoplasm of three independent replicates per arm from PDX model Gar15-13 following 10 days of treatment with vehicle (2% DMSO daily, green), NVP-CGM097 (50mg/kg daily, red), fulvestrant (5mg weekly, blue) or the combination of fulvestrant and NVP-CGM097 (purple). Tumours treated with fulvestrant alone or in combination had significantly reduced ER staining in both cellular compartments compared to tumours not treated with fulvestrant. Tumour cell identification and ER quantification were performed in QuPath software. **D.** Heat map of significant downregulated genes from the E2F Targets and G_2/M Checkpoint gene sets in the Gar1513 PDX model. **E.** Normalised $\log_2$ expression levels of significant p53 target genes in in the Gar1513 PDX model induced by NVP-CGM097 (red), fulvestrant (blue) and the combination of NVP-CGM097 and fulvestrant (purple), averaged by condition, associated with cell cycle, apoptosis and senescence.

Fig. S5. MDM2 inhibition in combination with CDK4/6 inhibition synergistically downregulates cell cycle markers *in vitro.*

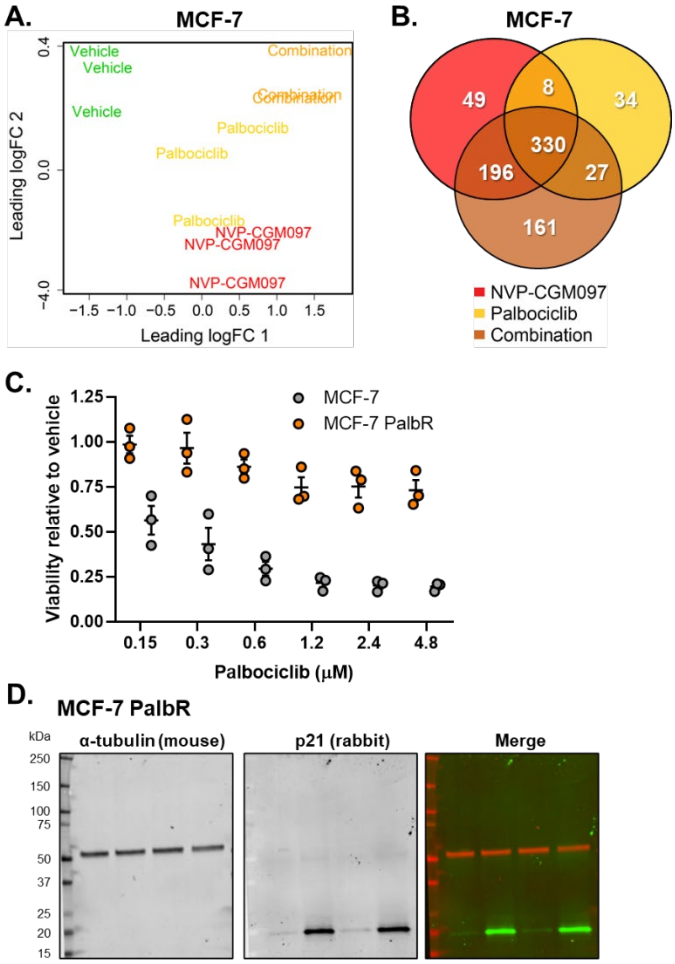

A. MDS plot of MCF-7 cell lines treated for 48h with Vehicle (0.01% DMSO), 1μM NVP-CGM097, 500nM palbociclib, or the combination of NVP-CGM097 and palbociclib. **B.** Venn diagram showing the overlap between differentially expressed genes (adjusted p-value < 0.05- and 2-fold change) induced by treatment in MCF-7 cell lines. **C.** Viability of parental MCF-7 (grey) and MCF-7 PalbR (orange) after treatment with the indicated dose of palbociclib for 72 hours. Values are shown relative to vehicle treated cells. **D.** Full gel images for the Western blots shown in Fig. 7D.